Semi-conservative transmission of DNA N^6-adenine methylation in a unicellular eukaryote

Yalan Sheng[1,2]†‡, Yuanyuan Wang[1,2]†, Wentao Yang[3]†, Xue Qing Wang[3], Jiuwei Lu[4], Bo Pan[1,2], Bei Nan[1,2], Yongqiang Liu[1,2], Fei Ye[1,2], Chun Li[5], Jikui Song[4], Yali Dou[3], Shan Gao[1,2*], Yifan Liu[3*]

[1]MOE Key Laboratory of Evolution and Marine Biodiversity and Institute of Evolution and Marine Biodiversity, Ocean University of China, Qingdao 266003, China

[2]Laboratory for Marine Biology and Biotechnology, Qingdao Marine Science and Technology Center, Qingdao 266237, China

[3]Department of Biochemistry and Molecular Medicine, Keck School of Medicine, University of Southern California, Los Angeles, CA 90033, USA

[4]Department of Biochemistry, University of California Riverside, Riverside, CA 92521, USA

[5]Division of Biostatistics, Department of Preventive Medicine, University of Southern California, Los Angeles, CA 90033, USA

†These authors contributed equally to this work

‡Present address: Guangzhou Key Laboratory of Subtropical Biodiversity and Biomonitoring, Guangdong Provincial Key Laboratory for Healthy and Safe Aquaculture, School of Life Sciences, South China Normal University, Guangzhou 510631, China

*Correspondence: shangao@ouc.edu.cn (S.G.); Yifan.Liu@med.usc.edu (Y.L.)

19 ## Running title

20 6mA semi-conservative transmission in eukaryotes

Abstract

While DNA N^6-adenine methylation (6mA) is best known in prokaryotes, its presence in eukaryotes has generated great interest recently. Biochemical and genetic evidence supports that AMT1, a MT-A70 family methyltransferase (MTase), is crucial for 6mA deposition in unicellular eukaryotes. Nonetheless, 6mA transmission mechanism remains to be elucidated. Taking advantage of Single Molecule Real-Time Circular Consensus Sequencing (SMRT CCS), here we provide definitive evidence for semi-conservative transmission of 6mA in *Tetrahymena thermophila*. In wild-type (WT) cells, 6mA occurs at the self-complementary ApT dinucleotide, mostly in full methylation (full-6mApT); after DNA replication, hemi-methylation (hemi-6mApT) is transiently present on the parental strand, opposite to the daughter strand readily labeled by 5-bromo-2'-deoxyuridine (BrdU). In Δ*AMT1* cells, 6mA predominantly occurs as hemi-6mApT. Hemi-to-full conversion in WT cells is fast, robust, and processive, while *de novo* methylation in Δ*AMT1* cells is slow and sporadic. In *Tetrahymena*, regularly spaced 6mA clusters coincide with linker DNA of nucleosomes arrayed in the gene body. Importantly, *in vitro* methylation of human chromatin by reconstituted AMT1 complex recapitulates preferential targeting of hemi-6mApT sites in linker DNA, supporting AMT1's intrinsic and autonomous role in maintenance methylation. We conclude that 6mA is transmitted by a semi-conservative mechanism: full-6mApT is split by DNA replication into hemi-6mApT, which is restored to full-6mApT by AMT1-dependent maintenance methylation. Our study dissects AMT1-dependent maintenance methylation and AMT1-independent *de novo* methylation, reveals a 6mA transmission

pathway with striking similarity to 5-methylcytosine (5mC) transmission at the CpG dinucleotide, and establishes 6mA as a *bona fide* eukaryotic epigenetic mark.

Key words

DNA N^6-adenine methylation (6mA), semi-conservative, unicellular eukaryote, AMT1 methyltransferase, maintenance methylation

Introduction

As a base modification, N^6-adenine methylation can occur in both RNA (referred to as m6A) and DNA (6mA). 6mA in eukaryotes has also long been known, but its widespread presence is only lately realized (Fu et al. 2015; Mondo et al. 2017; Wang et al. 2017; Bochtler and Fernandes 2021). 6mA studies in eukaryotes are complicated by varying abundance and divergent functions across species. In protists, green algae, and basal fungi, 6mA is abundant, enriched at the ApT dinucleotide, and associated with genes, all of which are consistent with its role as an epigenetic mark (Fu et al. 2015; Mondo et al. 2017; Wang et al. 2017; Luo et al. 2018; Beh et al. 2019; Wang et al. 2019). In animals, plants, and higher fungi, 6mA is scarce, promiscuous in its sequence context, and associated with silenced genomic regions (Greer et al. 2015; Zhang et al. 2015; Koziol et al. 2016; Liu et al. 2016; Wu et al. 2016; Liang et al. 2018; Wang et al. 2018; Xiao et al. 2018; Zhou et al. 2018; Lyu et al. 2022). In these organisms it remains controversial whether 6mA is an enzymatically deposited epigenetic mark; alternatively, the modified base, as a RNA breakdown product, is merely mis-incorporated into DNA (Schiffers et al. 2017; Musheev et al. 2020; Bochtler and Fernandes 2021; Liu et al. 2021a; Kong et al. 2022; Lyu et al. 2022). More rigorous application of cutting-edge technologies, like Single Molecule Real-Time Circular Consensus Sequencing (SMRT CCS) mentioned below, has the potential to further clarify the issue (Kong et al. 2022).

Methyltransferases (MTases) of the MT-A70 family are involved in N^6-adenine methylation in eukaryotes (Iyer et al. 2011; Iyer et al. 2016). They are classified into several clades with distinct structures and functions (Iyer et al. 2016; Wang et al. 2019). Two of these clades are represented by AMT1 (also known as MTA1) and AMT6/7

(MTA9-B/MTA9), which are part of the eukaryotic 6mA MTase complex first identified in the protist *Tetrahymena thermophila* (Beh et al. 2019; Wang et al. 2019). METTL4/DAMT-1 are members of another clade (Greer et al. 2015), but they lack the DPPW motif critical for catalysis and their status as *bona fide* 6mA MTases is still not supported by biochemical evidence (Iyer et al. 2011; Iyer et al. 2016; Beh et al. 2019; Wang et al. 2019). Critically, AMT1 and AMT6/7 homologues are only found in protists, green algae, and basal fungi, while METTL4/DAMT-1 homologues are mostly found in animals, plants, and higher fungi (Beh et al. 2019; Wang et al. 2019). Phylogenetic distributions of these two deep branches of MT-A70 family members therefore closely match that of the two alternative modes of 6mA in eukaryotes (Beh et al. 2019; Wang et al. 2019). However, even in the best characterized *Tetrahymena* system, molecular mechanisms of 6mA transmission still need to be elucidated.

Tetrahymena thermophila, a ciliated protist, is the first eukaryote with 6mA identified in its nuclear DNA (Gorovsky et al. 1973), and more recently, with AMT1, the eukaryotic 6mA-specific MTase, identified and characterized (Beh et al. 2019; Wang et al. 2019). *Tetrahymena* contains within the same cytoplasmic compartment two types of nuclei, the somatic macronucleus (MAC) and the germline micronucleus (MIC) (Karrer 2012). While missing in the transcriptionally silent MIC, 6mA is abundantly present in the transcriptionally active MAC and associated with RNA polymerase II-transcribed genes, consistent with its role as a euchromatic mark (Gorovsky et al. 1973; Wang et al. 2017).

6mA is readily detected by Single Molecule Real-Time (SMRT) sequencing via its perturbation to DNA polymerase kinetics—specifically increase in the time between nucleotide incorporation, referred to as the inter-pulse duration (IPD) (Fig. 1A) (Eid et al.

2009; Flusberg et al. 2010). Genome-wide mapping of endogenous 6mA in eukaryotes has previously been achieved only at the ensemble level, by combining different DNA molecules covering the same genomic position to overcome random fluctuations in IPD—an approach referred to as Continuous Long Reads (CLR) (Wang et al. 2017; Beh et al. 2019; Wang et al. 2019). Effective implementation of Circular Consensus Sequencing (CCS; also known as PacBio HiFi Sequencing), by combining reads from multiple passes of the same DNA template (Fig. 1B) (Eid et al. 2009; Flusberg et al. 2010; Wenger et al. 2019; Kong et al. 2022), allows us to accurately map 6mA distribution in the *Tetrahymena* MAC genome at the single molecule level and rigorously establish AMT1-dependent semi-conservative transmission of 6mA.

Results

6mA detection at the single molecule level

Recent development of SMRT CCS has allowed highly accurate and sensitive 6mA calling at individual DNA molecules. SMRT CCS has been applied to detect endogenous 6mA in several eukaryotes (Kong et al. 2022). However, very short inserts/reads (a few hundred bp) are used to maximize 6mA calling accuracy (high number of passes of the DNA template), but at the cost of genome-wide coverage. SMRT CCS has also been applied to detect exogenously introduced 6mA in chromatin fiber sequencing, which exploits *in vitro* methylation by 6mA-specific methyltransferases (e.g., M.EcoGII and Hia5) to probe the chromatin organization (Abdulhay et al. 2020; Stergachis et al. 2020). Long inserts/reads (~10 kb) are used to increase sequencing

coverage of large genomes of higher eukaryotes, but at the cost of reduced 6mA calling accuracy at individual DNA molecules (low number of passes of the DNA template). Here we developed a SMRT CCS-based pipeline to map 6mA on individual native DNA molecules from *Tetrahymena* (Supplemental Fig. S1A). Our analyses showed that at ≥ 30 passes, 6mA calling accuracy reached a plateau (Supplemental Fig. S1B). We therefore used intermediate sized inserts (3-5 kb, enabling most CCS reads to have ≥ 30 passes, given > 100 kb raw read length) to balance 6mA calling accuracy and sequencing coverage. We used the CCS read of a DNA molecule as its own reference sequence in the IPD analysis, yielding averaged and standardized IPD ratios (IPDr) for each site, relative to the *in silico* reference for its unmodified counterpart (Supplemental Fig. S1A) (Kong et al. 2022). A typical DNA molecule from wild-type (WT) *Tetrahymena* cells showed low IPDr for most adenine (A) sites and a few clusters with high IPDr (Fig. 1C). As most A sites are presumably unmodified, they formed a baseline of IPDr around 1, with low dispersion across the read length (Fig. 1C). As exceptions, we found DNA molecules with global anomalies in IPDr, whose baseline dispersed or deviated from 1 (Supplemental Fig. S1C, D), possibly due to a compromised DNA polymerase. We also found DNA molecules with local anomalies in IPDr, which contained one or more clusters of G/C/T sites with high IPDr as well as A sites (Supplemental Fig. S1E), attributable to DNA damage (Wenger et al. 2019). We removed reads with global or local anomalies in IPDr, to further improve 6mA calling accuracy.

We next mapped CCS reads back to the *Tetrahymena* MAC, MIC, and mitochondrion reference genomes (Supplemental Fig. S2A-D). Most were aligned across the entire read to a single genomic locus (Supplemental Fig. S2B). There were

some chimeric reads with different parts aligned to separate genomic loci (Supplemental Fig. S2B), attributable to concatenation during sequencing library preparation. Their constituent DNA molecules were resolved before further analysis (Supplemental Fig. S2C). For DNA molecules fully mapped to the MAC genome (Supplemental Fig. S2D), their IPDr for A sites exhibited a bimodal distribution: a large peak with low IPDr corresponding to unmodified A and a small peak with high IPDr corresponding to 6mA (Fig. 1D: top). A similar bimodal distribution was observed when we focused on A sites at the ApT dinucleotide (Fig. 1D: top). The 6mA peaks of these two distributions were almost superimposable (Fig. 1D: top, Supplemental Fig. S2E: left). In contrast, IPDr distributions of A sites within the ApA/ApC/ApG dinucleotides all exhibited a single peak with low IPDr (Fig. 1D: top). These analyses indicate that 6mA is exclusively associated with the ApT dinucleotide ($\frac{6\text{mApT}}{6\text{mA}}$ > 99%) (Supplemental Fig. S2E: left).

We deconvoluted the 6mA peak and unmodified A peak in the IPDr distribution for the ApT dinucleotide: the 6mA peak was closely fitted by a Gaussian distribution curve, while the unmodified A peak was deduced as the differential between the original data and the Gaussian fit (Fig. 1E: top). We set the threshold for 6mA calling at the intersection of the two peaks (IPDr=2.38) and estimated that the false positive and false negative rates of 6mApT calling were 1.93% and 1.12%, respectively (Fig. 1E: top). We calculated that 6mApT represented 1.89% of all ApT sites (and 6mA represented 0.66% of all A sites) in DNA molecules fully mapped to the MAC genome.

To validate our bioinformatic pipeline, we reanalyzed a published dataset of plasmid DNA sequenced by SMRT CCS (Abdulhay et al. 2020). We found that adenines in

GATC sites, uniformly methylated by *E. coli dam* MTase, were distributed in a single peak with high IPDr, while all other adenines were distributed in a single peak with low IPDr; the combined bimodal distribution is readily deconvoluted by our method, with low false positive and false negative rates (Supplemental Fig. S2F). Using the same IPDr threshold for reads mapped to the MAC, 6mApT was called only at low levels for DNA molecules specifically mapped to the MIC (0.017%) or mitochondrion (0.014%) (Supplemental Fig. S2G, Supplemental Table S1). 6mA was called at low levels at the ApC/ApG/ApA dinucleotides regardless of their mapping (Supplemental Table S1), which were close to the background level observed in the plasmid DNA negative control (Supplemental Table S2). We also sequenced a negative control sample generated by whole genome amplification (WGA) of *Tetrahymena* DNA (Supplemental Fig. S3), effectively removing all base modifications while preserving the sequence information. Using the same bioinformatic pipeline, we found that all A sites or A sites at the ApT dinucleotide were distributed in a single peak with low IPDr (Supplemental Fig. S3A, B). We calculated the false positive rate for 6mApT calling in *Tetrahymena* MAC genomic DNA (Supplemental Fig. S3C), which was very low (0.030%) and comparable to the background level observed in the MIC and mitochondrion. Based on the accurate calling of 6mA, we conclude that 6mA occurs exclusively at the ApT dinucleotide in the MAC.

Our conclusion disagrees with previous estimates of substantial 6mA in non-ApT dinucleotides (12%) based on SMRT CLR (Wang et al. 2017; Beh et al. 2019; Wang et al. 2019). We examined whether 6mApT genomic positions called by CCS were also called by CLR in our previous study (Wang et al. 2017). While SMRT CCS can call 6mA on individual reads/DNA molecules, SMRT CLR only calls 6mA at the ensemble

level, by combining different reads covering the same genomic position, and is therefore affected by both sequencing coverage and 6mA homogeneity. We found that at high 6mApT coverage (i.e., the number of reads in which 6mApT has been called in a genomic position), CLR calls converged with CCS calls (Supplemental Fig. S4A, B); in contrast, they diverged at low 6mApT coverage (Supplemental Fig. S4A). Also, as 6mA homogeneity decreased (from high 6mA fraction (> 80%), and intermediate (20-80%), to low (< 20%)), percentage of 6mA called by CLR in non-ApT dinucleotides (regarded as false positive, based on our CCS analysis) increased (0.6%, 9.8%, and 82.7%, respectively). We performed additional analyses to attribute the difference between CCS and CLR calls to the poor performance of CLR, showing high rates for both false positive and false negative (Supplemental Materials and Methods; Supplemental Fig. S4C-G).

Distinguishing four methylation states of ApT duplexes

SMRT CCS makes strand-specific 6mA calls, as the DNA polymerase alternately passes through the Watson strand (W, defined as the forward strand in the reference genome) and the Crick strand (C, reverse) of a DNA template (Fig. 1B) (Flusberg et al. 2010). For self-complementary ApT duplexes, we plotted their distribution according to IPDr values of A sites on W and C, respectively, and found four groups with diagonal symmetry, corresponding to four methylation states: full methylation, methylation only on W (hemi-W), methylation only on C (hemi-C), and no methylation (Fig. 2A-C). We demarcated these four groups and estimated that 89.3% methylated ApT duplexes were full methylation (full-6mApT), while 10.7% were hemi-methylation (hemi-6mApT) (Table 1, Fig. 2C: left, Fig. 2D: top; Supplemental Fig. S5). Importantly, consistent evaluation

of the full- and hemi-6mApT percentages was obtained in duplicate experiments (Supplemental Fig. S5) and with varying number of CCS passes (Supplemental Fig. S7). Our results establish the predominance of full-6mApT over hemi-6mApT in WT *Tetrahymena* cells, in contrast to the near parity assessment (54% and 46%, respectively) based on CLR (Wang et al. 2019). Note that only SMRT CCS can distinguish between hemi- and full-6mApT at the single molecule level, while CLR must extrapolate from the ensemble level.

We compared genomic positions to which hemi-6mApT and full-6mApT sites were mapped back and found a very strong overlap between them (> 99.9%) (Supplemental Fig. S6A). Furthermore, most genomic positions with multiple full-6mApT calls also contained multiple hemi-6mApT calls (Supplemental Fig. S6B). These observations support the interconversion between the hemi and full-methylation states at most genomic positions, we define 6mA penetrance for each genomic position as the ratio between the number of 6mA sites and all adenine sites (with or without the modification) mapped to it. For WT cells, 6mA penetrance for most ApT positions showed no significant bias for either W or C (Fig. 6D: top); with increasing sequencing coverage, 6mA penetrance from both strands tended to converge (Fig. 6D: middle). In other words, at the ensemble level, most ApT positions in the genome were methylated at similar levels on W or C. We did not observe biased 6mA penetrance in most asymmetrically methylated ApT positions reported previously (Wang et al. 2019), and attributed them as a CLR artifact (for exceptions, see **AMT1-independent *de novo* methylation**). Our result is consistent with DNA replication splitting a full-6mApT into a hemi-W and a hemi-C.

Segregation of hemi-6mApT to the parental strand after DNA replication

We next investigated segregation of hemi-W and hemi-C at the single molecule level. We focused on DNA molecules with multiple hemi-6mApT, henceforth referred to as hemi$^+$ molecules (Fig. 2D: top, Supplemental Fig. S6C, D). Their levels oscillated with cell cycle progression, starting low for cells synchronized in G1 phase, climbing to the peak for cells in S phase, and declining for post-replicative and dividing cells (Fig. 4A). In the vast majority of hemi$^+$ molecules, hemi-6mApT were not randomly distributed across both strands; instead, their constituent 6mA sites were segregated with a strong bias for one strand (Fig. 2D: top, Fig. 4B, C, and Supplemental Fig. S6D). Also, segregation strand bias was consistently observed with varying number of CCS passes (Supplemental Fig. S6). These robust results support hemi$^+$ molecules as the product of DNA replication. Segregation was not always absolute: a minority of hemi-6mApT were occasionally detected on the opposite strand (Supplemental Fig. S6D). This is most likely due to *de novo* methylation, either AMT1-dependent (see **AMT1-dependent maintenance methylation**) or AMT1-independent (see **AMT1-independent *de novo* methylation**).

We used 5-bromo-2'-deoxyuridine (BrdU) labeling to determine whether hemi-6mApT are segregated to the parental (old) strand or the daughter (newly synthesized) strand after DNA replication. We first set up an *in vitro* BrdU-labeling system (Fig. 3). Using a plasmid DNA fragment as the template, we performed specific labeling of either strand by primer extension, as well as total labeling of both strands by PCR (Fig. 3A). It is important to note that in the original plasmid DNA, there are three fully methylated GATC sites, which are readily converted to the hemi-methylated or unmethylated state

as either or both DNA strands are replaced during BrdU-labeling (Fig. 3A, B). We then performed SMRT CCS of these BrdU-labeled samples, as well as the unlabeled plasmid DNA as the negative control. We found that BrdU substitution of thymidine (T) resulted in IPDr increases, allowing us to adapt the 6mA calling pipeline for BrdU calling (Fig. 3B, C, Supplemental Fig. S8A-B). While there were a few T positions with large shifts in IPDr, most showed only small changes (Supplemental Fig. S8C-E). We applied a single high IPDr threshold for BrdU calling (IPDr=2.5), to achieve relatively low false positive rates (~5-10%; Fig. 3C), at the cost of high false negative rate (estimated >> 50% overall). To further increase the chance to correctly identify BrdU-labeled DNA molecules, we focused on those with multiple BrdU calls, henceforth referred to as $BrdU^+$ molecules (Fig. S8F). There were very few $BrdU^+$ molecules in unlabeled plasmid DNA, but many in BrdU-labeled samples (Fig. 3D, Supplemental Fig. S8F). Critically, in samples with strand-specific BrdU-labeling, BrdU calls were predominantly made on the labeled strand, but not on the unlabeled strand, as indicated by strong segregation strand bias of BrdU in $BrdU^+$ molecules (Fig. 3E, Supplemental Fig. S8G). These results validate our bioinformatic pipeline for BrdU calling and our use of BrdU-labeling for distinguishing the parental strand and the daughter strand.

We performed *in vivo* BrdU-labeling of *Tetrahymena* cells, sequenced the genomic DNA by SMRT CCS, and called BrdU as well as 6mA (Supplemental Fig. S9A, B). To eliminate interference from 6mA, we masked regions adjacent to 6mApT sites from BrdU calling (Supplemental Fig. S9B). We focused on $BrdU^+$ molecules (Fig. 4E, F). In BrdU-labeled samples, BrdU sites in $BrdU^+$ molecules were mostly segregated to one strand (Fig. 4E). In the unlabeled sample, “BrdU” sites were more evenly distributed

across both strands, consistent with miscalls due to random fluctuations in IPDr (Fig. 4E). Our approach was further validated by strong correlations between BrdU labeling and $BrdU^+$ molecules: ***1)*** there were many $BrdU^+$ molecules in BrdU-labeled samples, but few in the unlabeled sample (the percentage was further reduced when focusing on $BrdU^+$ molecules with strong biases in strand segregation); and ***2)*** the percentage of $BrdU^+$ molecules increased progressively with longer labeling time (Fig. 4F). BrdU segregation was often not absolute (Fig. 4E), attributable to false positive BrdU calls (Fig. 4D). Nonetheless, the large number of BrdU sites in $BrdU^+$ molecules allow us to identify the daughter strand with high confidence.

There was a significant overlap between $BrdU^+$ and $hemi^+$ molecules in BrdU-labeled samples (Supplemental Fig. S9C-F). We focused on $BrdU^+/hemi^+$ double-positive molecules representing post-replicative DNA (Fig. 4G, H). Critically, BrdU and hemi-6mApT always exhibited the opposite biases for strand segregation in $BrdU^+/hemi^+$ molecules (Fig. 4G, H). This result indicates that after DNA replication, hemi-6mApT is essentially excluded from the daughter strand and only associated with the parental strand.

AMT1-dependent maintenance methylation

To complete semi-conservative transmission of 6mA, hemi-6mApT needs to be restored to full-6mApT by maintenance methylation before the next round of DNA replication. We investigated whether maintenance methylation was dependent on AMT1. In Δ*AMT1* cells, SMRT CCS showed that 6mA was still predominantly associated with the ApT dinucleotide ($\frac{6\text{mApT}}{6\text{mA}}$ > 97%; Fig. 1D: bottom, Supplemental Fig. S2E: right), in

contrast to our previous estimation of a majority of 6mA in non-ApT dinucleotides (53%) based on SMRT CLR (Wang et al. 2019). While WT cells contained mostly full-6mApT (89%), there were few in Δ*AMT1* cells (3%) (Fig. 1E: bottom, Fig. 2B, Fig. 2C: right, Fig. 2D: bottom, Table 1). The predominant hemi-6mApT in Δ*AMT1* cells is presumably the product of a dedicated *de novo* MTase. We conclude that AMT1 is required for hemi-to-full conversion, *i.e.*, maintenance methylation.

AMT1 is part of a multi-subunit MTase complex (Beh et al. 2019; Chen et al. 2022; Yan et al. 2023). We next reconstituted AMT1 complex comprising bacterially expressed AMT1, AMT7, AMTP1, and AMTP2 (also known as MTA1, MTA9, p1, and p2 (Beh et al. 2019)) (Fig. 5A). Using a 12-bp DNA substrate with a single centrally located hemi-6mApT, we tested the reconstituted complex for *in vitro* methylation and evaluated its steady-state kinetics (K_m=0.55μM, k_{cat}=0.84min^{-1}; Fig. 5B). We also compared methylation rates of two 27-bp DNA substrates with the same primary sequence: the hemi-methylated substrate (with two 6mApT sites segregated to one strand) and the unmodified substrate (Fig. 5C). The hemi-methylated substrate recorded 11.5× higher activity than the unmodified substrate (Fig. 5C), a much bigger advantage than previously reported (Beh et al. 2019). AMT1 complex therefore strongly prefers maintenance methylation to *de novo* methylation.

We also performed *in vitro* methylation of human chromatin using the reconstituted AMT1 complex (Fig. 5D-G, Supplemental Fig. S10); as a control, we used M.EcoGII, a prokaryotic MTase targeting adenine sites in any sequence context (Murray et al. 2018). Due to scarcity of endogenous 6mA in human genomic DNA (O'Brown et al. 2019; Douvlataniotis et al. 2020; Bochtler and Fernandes 2021; Kong et al. 2022), all 6mA

sites revealed by SMRT CCS were essentially attributable to the added MTases. We found that 85% of 6mA sites were at the ApT dinucleotide after AMT1 complex treatment; only 22% of 6mA sites were so after M.EcoGII treatment, close to the ApT frequency in sequenced DNA molecules (Fig. 5D, E, Supplemental Fig. S10C). The substantial 6mA in non-ApT dinucleotides (15%) after AMT1 complex treatment is consistent with previous characterization of 6mA-MTase activity partially purified from *Tetrahymena* (Bromberg et al. 1982). Therefore, *in vitro* methylation catalyzed by AMT1 complex occurs preferentially at the ApT dinucleotide, but not exclusively, as *in vivo*.

Methylation of ApT sites was at similar levels and far from saturation in both AMT1 complex and M.EcoGII-treated samples ($\frac{6\text{mApT}}{6\text{mApT}+\text{ApT}}$=8.1% and 9.5%, respectively). However, 85% methylated ApT duplexes were full-6mApT after AMT1 treatment, while only 26% were so after M.EcoGII treatment (Fig. 5F, G). In the case of AMT1 complex, we found that the IPDr threshold for calling 6mA in ApT duplexes with 6mA on the opposite strand was substantially lowered, when compared with the IPDr threshold for calling 6mA in bulk ApT duplexes (conditional probability≠unconditional probability) (Fig. 5F: top). Importantly, a very similar shift in the IPDr threshold for calling 6mA in ApT duplexes was observed in WT *Tetrahymena* cells (Fig. 2C: left). In the case of M.EcoGII, the IPDr threshold for calling 6mA in ApT duplexes stayed the same, regardless of the methylation state of the opposite strand (conditional probability=unconditional probability) (Fig. 5F: bottom). Therefore, M.EcoGII does not prefer maintenance methylation (hemi-to-full conversion) over *de novo* methylation (un-to-hemi conversion); as a corollary, full-6mApT is generated by random combination of

two independent methylation events. In contrast, AMT1-dependent maintenance methylation is much faster than *de novo* methylation, leading to accumulation of full-6mApT and depletion of hemi-6mApT under *in vitro* as well as *in vivo* conditions. Therefore, preferential targeting of ApT, especially hemi-6mApT, is an intrinsic and autonomous property of AMT1 complex. We conclude that 6mA is transmitted by a semi-conservative mechanism in *Tetrahymena*: full-6mApT is split by DNA replication into hemi-6mApT, which is restored to full-6mApT by AMT1-dependent maintenance methylation (Fig. 5H).

Preferential methylation of linker DNA by AMT1 complex

Previous studies have shown that in unicellular eukaryotes, 6mA distribution is connected to nucleosome distribution, suggesting that 6mA transmission relies on the chromatin environment as well as the sequence context (Fu et al. 2015; Wang et al. 2017; Beh et al. 2019). SMRT CCS revealed that on individual DNA molecules from WT *Tetrahymena* cells, 6mA sites generally distributed in clusters separated by regular intervals (Fig. 6A). Autocorrelation analysis confirmed that 6mA sites were strongly phased at the single molecule level, oscillating with cycles of ~200bp (Fig. 6B). Furthermore, 6mA clusters from different DNA molecules were often coarsely aligned to the same genomic region (Fig. 6A). Indeed, 6mA distribution was also phased at the ensemble level (Fig. 6C: top), just like nucleosome distribution in *Tetrahymena* (Xiong et al. 2016). Autocorrelation analysis showed that 6mA and nucleosome distributions in *Tetrahymena* shared the same cycle of ~200bp (Fig. 6C: top); cross-correlation analysis showed that 6mA and nucleosome distributions were offset by ~100bp and in opposite phases (Fig. 6C: bottom). We also found that 6mA peaks coincided with nucleosome

368 troughs downstream of transcription start sites (Fig. 6A, Supplemental Fig. S10A).
369 Therefore, 6mA is preferentially associated with linker DNA in *Tetrahymena*.

370 We also analyzed human chromatin *in vitro* methylated by AMT1 complex or
371 M.EcoGII (Fig. 6D, E, Supplemental Fig. S10B-D). We first digested the DNA samples
372 with *Dpn*I (Supplemental Fig. S10A, B), targeting GATC sites with 6mA (Vovis and
373 Lacks 1977). Only a fraction of GATC sites were cleaved, generating a nucleosome
374 ladder strongly suggestive of preferential DNA methylation at linker DNA (Supplemental
375 Fig. S10B). SMRT CCS revealed regularly distributed 6mA clusters on individual DNA
376 molecules from both AMT1 complex and M.EcoGII-treated samples (Fig. 6D,
377 Supplemental Table S3). The difference in 6mA density is mostly due to much lower
378 density of the ApT dinucleotide that is preferred by AMT1, relative to essentially all A
379 sites that can be targeted by M.EcoGII. Autocorrelation analysis confirmed that 6mA
380 sites were strongly phased, with cycles ranging from 160 to 200bp (Fig. 6E: bottom).
381 DNA molecules with regularly spaced 6mA clusters were mapped across the entire
382 genome, in euchromatic and heterochromatic regions. While 6mA density was
383 substantially lower in the sample treated by AMT1 complex (Fig. 6D), the aggregated
384 6mA distribution correlogram showed the same cycle of ~190bp for both samples (Fig.
385 6E: top), underpinned by the nucleosome distribution pattern in human chromatin.

386 In contrast to *Tetrahymena* MAC genomic DNA, 6mA clusters on different DNA
387 molecules from *in vitro* methylated human chromatin were poorly aligned for most
388 genomic regions (Fig. 6D). Indeed, 6mA distribution autocorrelation was much weaker
389 for *in vitro* methylated human chromatin at the ensemble level (Supplemental Fig.
390 S11A). In parallel, autocorrelation for nucleosome distribution at the ensemble level

391 was much weaker in human than in *Tetrahymena*, indicating poor nucleosome
392 positioning overall in human relative to *Tetrahymena* (Fig. 6C: top, Supplemental Fig.
393 S11B). As an exception that proves the rule, we found that around genomic positions
394 with strong CTCF-binding, which are usually flanked by well-positioned nucleosomes
395 (Fu et al. 2008; Krietenstein et al. 2020), 6mA sites from *in vitro* methylated human
396 chromatin were strongly aligned, and importantly, 6mA peaks coincided with
397 nucleosome troughs (Supplemental Fig. S11C). We conclude that mutual exclusivity
398 between 6mA and the nucleosome is generally applicable at the single molecule level,
399 but only manifests at the ensemble level for genomic regions with well-positioned
400 nucleosomes. Our *in vitro* methylation results also indicate that preferential methylation
401 of linker DNA is an intrinsic property for AMT1 complex, M.EcoGII, and potentially many
402 other MTases.

403 ## Processivity of AMT1-dependent methylation

404 Canonical maintenance MTases (*e.g.*, *E. coli* dam DNA MTase) are generally
405 processive rather than distributive (Urig et al. 2002). In other words, upon substrate
406 binding, they tend to catalyze multiple local methylation events before dissociation. To
407 investigate processivity of AMT1-dependent methylation, we examined DNA molecules
408 undergoing hemi-to-full conversion in WT *Tetrahymena* cells. We found that hemi-
409 6mApT and full-6mApT distributions were often not random in these molecules (Fig. 6F-
410 I). Many exhibited full-6mApT congregation: the maximum observed distance between
411 adjacent full-6mApT positions (max inter-full distances) was much smaller than
412 expected, and as a result rarely appeared in simulated controls, in which full-6mApT
413 and hemi-6mApT positions were randomly permutated (Fig. 6F). There was a strong

tendency for multiple maintenance methylation events to occur in nearby positions. This tendency was especially prominent for DNA molecules early in the hemi-to-full conversion process, which were more likely to be methylated in a processive run by a single AMT1 complex (Supplemental Fig. S12A).

For DNA molecules with strong full-6mApT congregation, their max inter-full distances were predominantly distributed in two peaks (Fig. 6G): the left peak (max inter-full distances ≤ 30bp) corresponds to full-6mApT congregation within the same linker DNA (Fig. 6H), while the right peak (130bp ≤ max inter-full distances ≤ 200bp) corresponds to congregation across adjacent linker DNA regions (Fig. 6I). Consistent with chromatin-guided 6mA transmission, in some DNA molecules, hemi-to-full conversion was already complete for one linker DNA (or at a higher level, gene), but not even started for its adjacent linker DNA region (or gene) (Fig. 6H, I). More often, full-6mApT were intermixed with hemi-6mApT in one linker DNA region (or gene), while its adjacent linker DNA region (or gene) contained only hemi-6mApT (Supplemental Fig. S12B). The processivity of AMT1-dependent maintenance methylation therefore manifests as episodes of hemi-to-full conversion events that occur within one linker DNA (or gene), punctuated by switching of the MTase activity to its adjacent linker DNA (or gene).

AMT1-independent *de novo* methylation

6mA levels were reduced but not eliminated in Δ*AMT1* cells (Table 1). Many ApT positions in the MAC genome were methylated in WT cells but not in Δ*AMT1* cells (Supplemental Fig. S13A). For genomic positions methylated in both, methylation

436 penetrance was generally much lower in Δ*AMT1* cells (Supplemental Fig. S13B). High
437 penetrance genomic positions were especially depleted in Δ*AMT1* cells (Fig. 7A).
438 Assuming exponential decay kinetics, we estimated the apparent half-life values for
439 AMT1-dependent maintenance methylation (0.07× cell cycle) and AMT1-independent
440 *de novo* methylation (17.6×) (Supplemental Fig. S14). The fast AMT1-dependent
441 maintenance methylation allows effective restoration of full-6mApT within one cell cycle
442 in WT cells, while the slow AMT1-independent *de novo* methylation entails that in
443 Δ*AMT1* cells, methylation plateau is only reached after multiple cell cycles. Indeed, in
444 many DNA molecules from Δ*AMT1* cells, 6mA counts on W and C were disparate (Fig.
445 2D: bottom, Fig. 7B, Supplemental Fig. S13C-D). The strand with significantly fewer
446 6mA than expected for random distribution probably corresponds to the daughter strand
447 after DNA replication, which only carries 6mA newly deposited after the last S phase;
448 the strand with significantly more 6mA probably corresponds to the parental strand,
449 which has accumulated 6mA over multiple cell cycles. The difficulty to propagate 6mA
450 across the cell cycle also led to epigenetic instability in Δ*AMT1* cells, as different DNA
451 molecules covering the same gene exhibited much higher variability of 6mA counts (Fig.
452 7C).

453 In Δ*AMT1* cells, 6mA was also enriched in linker DNA and towards the 5' end of Pol
454 II-transcribed genes (Supplemental Fig. S15A, B). 6mApT sites, though present more
455 sparsely, still formed clusters at regular intervals on individual DNA molecules (Fig. 2D:
456 bottom, Supplemental Fig. S15B). Autocorrelation analysis at both the single molecule
457 level and the ensemble level showed a slight right shift in 6mA peaks, supporting
458 increased linker DNA length (Supplemental Fig. S15C-E). We found many genomic

regions that were more variably covered with 6mA in Δ*AMT1* than WT cells (Supplemental Fig. S15B). This may reflect reduced nucleosome positioning or increased nucleosome dynamics. In support, 6mA can directly promote nucleosome positioning, as the heavily methylated DNA becomes less bendable and thus prefers to be linker DNA rather than nucleosomal DNA (Fu et al. 2015; Luo et al. 2018; Beh et al. 2019). Nucleosome positioning was indeed weakened in Δ*AMT1* relative to WT cells (Supplemental Fig. S15E) (Wang et al. 2019). Alternatively, 6mA dispersion in Δ*AMT1* cells may be attributed to the slow AMT1-independent *de novo* methylation, which records nucleosome movement over much longer period rather than only briefly after DNA replication.

In strong contrast to WT cells, 6mA penetrance for most ApT positions in the MAC genome of Δ*AMT1* cells showed strong biases for either W or C, and many were exclusively methylated on one strand (Fig. 2D: bottom, Fig. 7D: top); this tendency grew in prominence with increasing sequencing coverage (Fig. 7D: bottom), thus unlikely an artifact of random fluctuations. We also noted a very small minority of ApT positions containing predominantly, if not exclusively, hemi-methylation calls in WT *Tetrahymena* cells (Supplemental Fig. S6A: hemi-only part of the Venn diagram, 0.36%). These positions, characterized by a strong penetrance strand bias, were most likely methylated by an AMT1-independent *de novo* methylation pathway (Fig. 7E: left, Fig. 7F: Group 1). In the high copy number *Tetrahymena* rDNA, we found genomic positions that were exclusively targeted by AMT1-indpendent *de novo* methylation (Fig. 7E: left; Fig. 7F: Group 1), as well as those that were AMT1-dependent (Fig. 7E: right; Fig. 7F: Group 2). Genomic positions with strong penetrance bias for W or C exhibited periodic

distributions with a ~10-bp cycle (Figure 7G: top). This matches the pitch of the DNA double helix, suggesting that the dedicated *de novo* MTase is constrained to approach the DNA substrate from only one side (Figure 7G: right). The strong penetrance bias also precludes this MTase from playing a major role in maintenance methylation.

Despite these distinctions, there were also connections between AMT1-dependent and AMT1-independent methylation. Most ApT positions methylated in Δ*AMT1* cells were also methylated in WT cells; the two sets essentially converged at high methylation penetrance (Figure 7H, Supplemental Fig. S15A). Furthermore, 6mA levels at individual genes and even individual linker DNA regions of a gene showed strong correlations between WT and Δ*AMT1* cells (Figure 7I and S15E). These connections suggest an integrated 6mA transmission pathway: AMT1-independent *de novo* methylation primes the system by laying down an incipient 6mApT distribution pattern, which is fulfilled and transmitted by AMT1-dependent maintenance methylation.

Discussion

6mA detection by SMRT CCS

In the free 6mA nucleotide, N^6-methyl group minimizes the steric clash by pointing towards the Watson-Crick edge of the purine ring (Bochtler and Fernandes 2021). This is likely also the preferred conformation in single-stranded DNA. However, in double-stranded DNA, N^6-methyl group must adopt the energetically less favorable conformation and point the other way, to allow the N^6-lone pair electrons to engage in Watson-Crick base pairing. This entails a pause in DNA synthesis, as the DNA

polymerase waits for 6mA in the template strand to switch conformation. In SMRT sequencing, this is recorded as increased IPD. SMRT CCS allows robust evaluation of IPD at the single site and single molecule level, as multiple passes by the DNA polymerase overcome random fluctuations. We rationalize that 6mA and unmodified A feature distinct IPDr distributions, which can be deconvoluted effectively. Based on these basic assumptions, we have developed a bioinformatic pipeline to fully exploit the recent progress in SMRT CCS for strand-specific, accurate, and sensitive detection of 6mA on individual DNA molecules multi-kb in length. The result is the first high quality, single molecule, genome-wide mapping of endogenous 6mA in eukaryotes.

6mA detection by SMRT CCS is critical for our study in the following aspects. First, SMRT CCS detects 6mA with high accuracy (low false positive rates), which allows us to ***1)*** determine the ApT specificity for AMT1-dependent maintenance methylation and AMT1-independent *de novo* methylation, and ***2)*** distinguish hemi-6mApT from full-6mApT in WT and Δ*AMT1* cells. Second, SMRT CCS preserves long-range connectivity information at the single molecule level, which allows us to ***1)*** identify hemi^{+}/BrdU^{+} molecules and establish segregation of hemi-6mApT to the parental strand after DNA replication, and ***2)*** identify DNA molecules undergoing maintenance methylation and characterize AMT1 processivity. Third, SMRT CCS detects 6mA with high sensitivity (low false negative rates), which, combined with deep sequencing coverage of the *Tetrahymena* MAC genome, allows us to ***1)*** unambiguously identify rare methylation events, and ***2)*** to generate absolute and exact quantification of 6mA levels over a genomic region. Furthermore, there is gross discrepancy between CLR and CCS-based assessments of many key 6mA parameters in *Tetrahymena* cells, including

527 percentage of 6mA in non-ApT context, percentage of hemi- and full-6mApT, and
528 percentage of ApT positions with 6mA penetrance bias. In many cases, the misleading
529 CLR results are likely rooted in heterogeneity of 6mA at the single molecule level, which
530 cannot be readily reduced to a single-value representation at the ensemble level. Lastly,
531 although it has long been implicated and assumed that 6mA is transmitted by a semi-
532 conservative mechanism in eukaryotes, our novel application of SMRT CCS in this work
533 represents the first systematic and rigorous proof.

534 As a gold standard for 6mA detection, SMRT CCS boasts some outstanding
535 features: ***1)*** low background noise, ***2)*** high accuracy, ***3)*** high sensitivity, and ***4)*** long read
536 length. It is worth noting that these parameters are mutually connected and can be
537 individually optimized according to one's need. At the cost of CCS read length/DNA
538 insert size (and consequently, sequencing coverage), we chose to increase the number
539 of CCS passes to improve the first three parameters. Shifting IPDr threshold for 6mA
540 calling affects accuracy and sensitivity of 6mA detection in the opposite direction. Our
541 deconvolution-based approach automatically sets the threshold to achieve a balanced
542 outcome. SMRT CCS can be used to detect other base modifications, such as BrdU.
543 While we have limited ourselves to a single readout of the DNA polymerase kinetics
544 (IPD) and a rationally designed algorithm (independent of ground truth training data),
545 there is great potential in incorporating additional readout and implementing neural
546 network-based machine learning algorithms (Tse et al. 2021).

547 6mA is highly enriched in linker DNA in *Tetrahymena*. The resulting 6mA clusters,
548 regularly spaced, demarcate individual nucleosomes on a chromatin fiber, providing
549 long-range epigenetic information generally missing from short-read sequencing data.

Specific methylation of linker DNA is likely an intrinsic feature of AMT1 complex, M.EcoGII, and many other 6mA-MTases. This property can be exploited to probe chromatin organization via *in vitro* methylation, analogous to nuclease protection (Abdulhay et al. 2020; Shipony et al. 2020; Stergachis et al. 2020; Altemose et al. 2022). This is an especially powerful approach when combined with 6mA detection by SMRT CCS (Abdulhay et al. 2020; Stergachis et al. 2020).

AMT1-dependent methylation

We have extensively characterized AMT1-dependent 6mA transmission. Our *in vivo* results demonstrate high specificity for maintenance methylation at the ApT dinucleotide, while our *in vitro* results support substantial *de novo* methylation activity at ApT sites and, to a lesser degree, non-ApT sites. Note that 6mA at non-ApT sites is necessarily the product of *de novo* methylation. We emphasize that *de novo* methylation underpins the biochemical assay by which the *Tetrahymena* MTase activity and eventually AMT1 complex were identified (Bromberg et al. 1982; Beh et al. 2019). Indeed, DNMT1, the eukaryotic maintenance MTase required for semi-conservative transmission of 5-methylcytosine (5mC) in the CpG dinucleotide, also has *de novo* methylation activity (Bestor 2000; Jeltsch 2006). We argue that AMT1-dependent *de novo* methylation is amplified under *in vitro* conditions, while curtailed by various *in vivo* circumstances. ***1)*** For *in vitro* methylation of human chromatin, *de novo* methylation precedes—and is the prerequisite for—maintenance methylation. In contrast, the abundance of hemi-6mApT in *Tetrahymena* MAC DNA immediately after DNA replication allows maintenance methylation to effectively outcompete *de novo* methylation *in vivo*. ***2)*** Processivity of AMT1-dependent methylation may enhance the preference for maintenance methylation

in vivo. Multiple hemi-6mApT sites, present in a cluster often fully covering a linker DNA, are readily converted to full-6mApT with little chance of *de novo* methylation as the side reaction. ***3)*** AMT1-dependent maintenance methylation may be further enhanced by other *in vivo* factors. In *Tetrahymena*, 6mA is highly enriched in linker DNA flanked by nucleosomes containing H3K4me3 and H2A.Z (Wang et al. 2017), which may interact with AMT1 complex and modulate its substrate specificity.

Comparing 6mA and 5mC pathways in eukaryotes

Our work provides definitive evidence for a eukaryotic 6mA pathway comprising two distinct but linked steps: AMT1-independent *de novo* methylation and AMT1-dependent maintenance methylation (Fig. 8). While AMT1-independent *de novo* methylation is dispensable for maintaining the 6mA pattern in the MAC of asexually propagating *Tetrahymena* cells (Wang et al. 2019), it is likely to play a critical role during sexual reproduction, as the transcriptionally silent and 6mA-free germline MIC is differentiated into the transcriptionally active and 6mA-rich somatic MAC. This two-step pathway bears some striking resemblance to the eukaryotic 5mC pathway, featuring the DNMT3A/3B-dependent *de novo* methylation and DNMT1-dependent maintenance methylation for transmission of 5mC at the CpG dinucleotide (Fig. 8) (Goll and Bestor 2005; Lister et al. 2009; Sen et al. 2021). As *bona fide* eukaryotic epigenetic marks, 6mA and 5mC play opposite roles in transcription regulation (Fig. 8). Their transmission pathways are deep-rooted and widespread, but show distinct phylogenetic distributions, with homologues of AMT1 complex components notably missing from land plants, higher fungi, and animals (Supplemental Fig. S16). 6mA and 5mC therefore represent a pair of critical switches that can alter the global epigenetic landscape for transcription

596 regulation, and their presence or loss may drive some major branching events in
597 eukaryotic evolution.

598

Materials and Methods

Tetrahymena strains

Tetrahymena thermophila WT strain (SB210) was obtained from the *Tetrahymena* Stock Center. Δ*AMT1* was a homozygous homokaryon (MAC and MIC) knockout strain generated in our previous study (Wang et al. 2019). The knockout construct is available at Addgene (plasmid # 218373).

In vitro and *in vivo* BrdU-labeling

For *in vitro* BrdU-labeling, a *Pvu*I-digested fragment of the pBluescript II SK(-) plasmid (~1kb) was used as the template for primer extension and PCR. For PCR: Taq DNA polymerase, primers (PSK-Fwd: 5′- CGT TGT CAG AAG TAA GTT GGC CGC -3′; PSK-Rev: 5′- CGC CCT TCC CAA CAG TTG CGC -3′), and dNTP mix ($\frac{BrdUTP}{BrdUTP+TTP}$= 50% or 90%). For primer extension: Taq DNA polymerase, either PSK-Fwd or PSK-Rev, and dNTP mix ($\frac{BrdUTP}{BrdUTP+TTP}$= 90%). SMRT sequencing was performed on five samples: unlabeled plasmid, PSK-Fwd primer extension, PSK-Rev primer extension, 50% BrdUTP PCR, and 90% BrdUTP PCR.

For *in vivo* BrdU-labeling, *Tetrahymena* cells were synchronized at G1 phase by centrifugal elutriation (Liu et al. 2021b), released into the fresh medium with 0.4mM BrdU, and collected after 0h, 1.5h, 2h, or 4h for genomic DNA extraction and SMRT sequencing.

DNA methyltransferase assay of reconstituted AMT1 complex

Synthesized 12-mer DNA oligos containing one central 6mA-modified ApT site were annealed to generate the substrate (upper strand: 5′- GCA AG (6mA) TCA ACG -3′, lower stand: 5′- CGT TGA TCT TGC -3′). For steady-state kinetic assay, a 20µL reaction mixture contained the hemi-methylated substrate at various concentrations (0, 0.04, 0.1, 0.16, 0.24, 0.36, 0.5, 0.75, 1, 1.5, 2µM), 0.01µM AMT1 complex, 0.55µM S-adenosyl-L-[methyl-^{3}H] methionine (specific activity 18Ci/mmol, PerkinElmer), 1.9µM AdoMet in 50mM Tris–HCl, pH 8.0, 0.05% β-mercaptoethanol, 5% glycerol, and 200µg/mL BSA. For substrate specificity assay, a 15µL reaction mixture contained 2µM unmodified or hemi-methylated substrates, 0.1µM AMT1 complex, 3µM S-adenosyl-L-[methyl-^{3}H] methionine (specific activity 18Ci/mmol, PerkinElmer). For unmodified DNA duplex, upper strand: 5′- AAC TTC TGT CAT TAC ATT AAG CTT TAA -3′, lower stand: 5′- TTA AAG CTT AAT GTA ATG ACA GAA GTT -3′. For hemi-methylated DNA duplex, upper strand: 5′- AAC TTC TGT C (6mA) T TAC (6mA)TT AAG CTT TAA -3′, lower stand: 5′- TTA AAG CTT AAT GTA ATG ACA GAA GTT -3′. The assays were performed in triplicate at room temperature for 30 min.

In vitro methylation of human chromatin

1.7×10^{5} OCI-AML3 cells were lysed in 0.5 mL of nuclei extraction buffer (20mM HEPES pH 7.9, 10mM KCl, 0.1% Triton X-100, 20% glycerol, 0.5mM spermidine, 1× Protease Inhibitor Cocktail) for 8 min on ice. Purified nuclei were methylated in a 30µL of 50mM Tris-HCl pH 8.0, 2mM EDTA, 0.5mM EDGA, 160µM SAM, 1× Protease Inhibitor Cocktail and 38µM AMT1-complex or M.EcoGII or no enzyme control for 1h at 37°C. Genomic DNA was extracted with Monarch® HMW DNA Extraction Kit for Cells & Blood

(New England Biolabs), digested with *Dpn*I overnight at 37°C, and resolved on 1% agarose gel. DNA fragments 3-5kb in length were gel purified for SMRT sequencing.

SMRT CCS detection of 6mA

Native genomic DNA was extracted from *Tetrahymena* WT (SB210, with or without BrdU-labeling) and Δ*AMT1* cells using Wizard® Genomic DNA Purification Kit (Promega). REPLI-g Single Cell Kit (Qiagen) was used for whole genome amplification (negative control). DNA samples were sheared to 3-5kb in length with Megaruptor (Diagenode Diagnostics) and prepared for sequencing by the Sequel II System.

Single molecule SAM files were extracted from the SMRT sequencing data using custom Perl script and transformed into single molecule BAM files by SAMtools (Li et al. 2009). Circular Consensus Sequence (CCS) was calculated for each DNA molecule using the CCS module (SMRT Link v10.2, Pacific Biosciences). Only DNA molecules with high subread coverage (≥ 30×) were retained. Single molecule aligned BAM files were generated using BLASR (Chaisson and Tesler 2012), which in turn served as the input for the ipdSummary module to calculate IPD ratios (IPDr). Self-referencing not only allows 6mA calling at the single molecule level, but also greatly speeds up computation. We aligned CCS reads to the latest *Tetrahymena* genome references for the MAC (Sheng et al. 2020), MIC (Supplemental File_Tet MIC, updating the published MIC reference (Hamilton et al. 2016)), and mitochondrion (Brunk et al. 2003). All custom scripts and code were uploaded in the Supplemental_code. Additional details are available in Supplemental Methods “SMRT CCS data analysis”, “Mapping CCS reads back to genome references”, and “CCS versus CLR”.

SMRT CCS detection of BrdU

For analyzing *in vitro* BrdU-labeled DNA, SMRT CCS reads with high passes (≥60x) were aligned to the reference sequence using BLASTN, and only molecules satisfying a strict criterion of 0 mismatches, 0 gaps and an alignment length exceeding 1000bp were analyzed. Furthermore, strand-specific IPDr standard deviations (SD) of guanine sites (presumably all unmodified) were calculated and molecules with SD ≤ 0.35 for both strands were retained. The threshold for calling BrdU was set at an IPDr value of 2.5 or 2.8. $BrdU^+$ molecules were defined as DNA molecules with no less than 8 BrdU sites on one strand (W||C ≥ 8).

For analyzing *in vivo* BrdU-labeled *Tetrahymena* genomic DNA, regions adjacent to 6mApT sites (both strands: -10 to +10bp) were masked from BrdU calling to avoid interference between 6mA and BrdU. IPDr 2.8 was set as the threshold for calling BrdU. Note that $BrdU^+$ molecules, defined as DNA molecules with no less than 11 BrdU sites in total (W+C ≥ 11) or on one strand (W||C ≥ 11), represent a small fraction of BrdU-labeled DNA molecules (only ~10% of SMRT CCS reads were $BrdU^+$ in G2 cells, in which nearly all DNA should be labeled by BrdU), due to the high false negative rate of BrdU calls and the high threshold for $BrdU^+$ molecules.

Penetrance strand bias and segregation strand bias

6mA penetrance strand bias, $(\frac{W-C}{W+C})_p$, is defined for an ApT position in the genome as the difference-sum ratio between the number of DNA molecules supporting 6mA on W and C, respectively (W+C ≥ 10). The values range between -1 (6mA only on C) and 1 (6mA

only on W). 6mA penetrance strand bias was calculated for both WT and Δ*AMT1* cells. We identified ApT positions with penetrance strand bias of +1 or -1 in Δ*AMT1* cells and generated phasogram (defined as histogram of distances between specified positions) to reveal their periodic distribution relative to each other.

6mA segregation strand bias, $(\frac{W-C}{W+C})_s$, is defined for a hemi$^+$ molecule (W+C ≥ 11 or W||C ≥ 11) as the difference-sum ratio between the count of hemi-6mApT on W and C, respectively. The values range between -1 (only hemi-C) and 1 (only hemi-W). Note that 6mA in full-6mApT is not included in this calculation. Segregation strand bias is also calculated for BrdU sites in BrdU$^+$ molecules (W+C ≥ 15 or W||C ≥ 15).

Autocorrelation and cross-correlation analysis

A vector consisting of a series of 0's (no 6mA) and 1's (6mA at the position on either strand) was encoded for each DNA molecule with 6mA sites (≥ 2). This vector was the input for the acf function in the statsmodel Python package (Seabold et al. 2010) for computing 6mA autocorrelation coefficients at the single molecule level. For correlation analysis at ensemble level, the MAC reference genome was divided into 5kb regions. We then used BEDTools coverage subcommand (Quinlan and Hall 2010) to count 6mA or nucleosome dyad across all genomic positions, generating two encoding vectors for each such genomic region (focusing on genomic positions with 6mApT coverage ≥ 2; 6mApT genomic positions supported by only one 6mA call are excluded to reduce background noise). This pair of vectors were the input for the acf function for computing the autocorrelation coefficients of 6mA and nucleosome distributions, respectively; they were also the input for the ccf function for computing the cross-correlation coefficients

between 6mA and nucleosome distributions.

Full-6mApT congregation

For each DNA molecule undergoing hemi-to-full conversion (full-6mApT ≥ 3, hemi-6mApT ≥ 9), we first calculated the observed maximum value of distances between adjacent full-6mApT duplexes (D_{obs}). We then calculated the equivalent values for 1000 simulations, in which the full-6mApT and hemi-6mApT positions in the same DNA molecule were randomly permutated (D_{sim}). This allowed us to estimate the probability for observed full-6mApT congregation ($D_{sim} \leq D_{obs}$), assuming that maintenance methylation is random.

Data Access

The SMRT CCS data generated in this study have been submitted to the NCBI BioProject database (https://www.ncbi.nlm.nih.gov/bioproject/) under the accession number PRJNA932808.

Competing interests: None.

Acknowledgments

Tetrahymena WT strains were obtained from the *Tetrahymena* Stock Center (http://tetrahymena.vet.cornell.edu). SMRT sequencing was performed at the Genomics Core Facility, Icahn School of Medicine at Mount Sinai and Novogene Co., Ltd. (Beijing, China). High-performance computing resources for data processing were provided by the Institute of Evolution and Marine Biodiversity at Ocean University of

China, the Center for High Performance Computing and System Simulation at Laoshan Laboratory, Marine Big Data Center of Institute for Advanced Ocean Study at OUC, and the Center for Advanced Research Computing (CARC) at the University of Southern California.

Funding: National Natural Science Foundation of China 32125006, 32070437 (S.G.), National Natural Science Foundation of China 32200336 (Y.S.), National Natural Science Foundation of China 32200399 (Y.W.), Department of Biochemistry and Molecular Medicine at University of Southern California (Y.L.).

Author contributions: Yifan L. and S.G. conceived the project, supervised most of the experiments and data analyses, and prepared the manuscript. Y.S. and W.Y. analyzed SMRT CCS data. Y.W. set up *in vitro* and *in vivo* BrdU-labeling system and performed the *Tetrahymena* experiments. J.L. (supervised by J.S.) and B.N. (supervised by S.G.) reconstituted and characterized AMT1 complex, which was used by X.Q.W. (supervised by Y.D.) to perform *in vitro* methylation of the human chromatin. Yongqiang L. provided the synchronized *Tetrahymena* cells. F.Y. calculated the conversion rate of WT and Δ*AMT1* cells. B.P. analyzed Illumina sequencing data and phylogenetic distribution of DNA MTases. C.L. performed statistical analyses.

References

Abdulhay NJ, McNally CP, Hsieh LJ, Kasinathan S, Keith A, Estes LS, Karimzadeh M, Underwood JG, Goodarzi H, Narlikar GJ et al. 2020. Massively multiplex single-molecule oligonucleosome footprinting. *eLife* **9**: e59404.

Altemose N, Maslan A, Smith OK, Sundararajan K, Brown RR, Mishra R, Detweiler AM, Neff N, Miga KH, Straight AF et al. 2022. DiMeLo-seq: a long-read, single-molecule method for mapping protein-DNA interactions genome wide. *Nat Methods* **19**(6): 711-723.

Beh LY, Debelouchina GT, Clay DM, Thompson RE, Lindblad KA, Hutton ER, Bracht JR, Sebra RP, Muir TW, Landweber LF. 2019. Identification of a DNA N^6-adenine methyltransferase complex and its impact on chromatin organization. *Cell* **177**(7): 1781-1796.

Bestor TH. 2000. The DNA methyltransferases of mammals. *Hum Mol Genet* **9**(16): 2395-2402.

Bochtler M, Fernandes H. 2021. DNA adenine methylation in eukaryotes: enzymatic mark or a form of DNA damage? *Bioessays* **43**(3): e2000243.

Bromberg S, Pratt K, Hattman S. 1982. Sequence specificity of DNA adenine methylase in the protozoan *Tetrahymena thermophila*. *J Bacteriol* **150**(2): 993-996.

Brunk CF, Lee LC, Tran AB, Li J. 2003. Complete sequence of the mitochondrial genome of *Tetrahymena thermophila* and comparative methods for identifying highly divergent genes. *Nucleic Acids Res* **31**(6): 1673-1682.

Chaisson MJ, Tesler G. 2012. Mapping single molecule sequencing reads using basic local alignment with successive refinement (BLASR): application and theory. *BMC Bioinform* **13**(1): 238.

Chen J, Hu R, Chen Y, Lin X, Xiang W, Chen H, Yao C, Liu L. 2022. Structural basis for MTA1c-mediated DNA N^6-adenine methylation. *Nat Commun* **13**(1): 3257.

Douvlataniotis K, Bensberg M, Lentini A, Gylemo B, Nestor CE. 2020. No evidence for DNA N (6)-methyladenine in mammals. *Sci Adv* **6**(12): eaay3335.

Eid J, Fehr A, Gray J, Luong K, Lyle J, Otto G, Peluso P, Rank D, Baybayan P, Bettman B et al. 2009. Real-time DNA sequencing from single polymerase molecules. *Science* **323**(5910): 133-138.

Flusberg BA, Webster DR, Lee JH, Travers KJ, Olivares EC, Clark TA, Korlach J, Turner SW. 2010. Direct detection of DNA methylation during single-molecule, real-time sequencing. *Nat Methods* **7**(6): 461-465.

Fu Y, Luo GZ, Chen K, Deng X, Yu M, Han D, Hao Z, Liu J, Lu X, Dore LC et al. 2015. N^6-methyldeoxyadenosine marks active transcription start sites in *Chlamydomonas*. *Cell* **161**(4): 879-892.

778 Fu Y, Sinha M, Peterson CL, Weng Z. 2008. The insulator binding protein CTCF positions 20
779 nucleosomes around its binding sites across the human genome. *PLoS Genet* **4**(7):
780 e1000138.

781 Goll MG, Bestor TH. 2005. Eukaryotic cytosine methyltransferases. *Annu Rev Biochem* **74**: 481-
782 514.

783 Gorovsky MA, Hattman S, Pleger GL. 1973. (^{6}N)methyl adenine in the nuclear DNA of a
784 eucaryote, *Tetrahymena pyriformis*. *J Cell Biol* **56**(3): 697-701.

785 Greer EL, Blanco MA, Gu L, Sendinc E, Liu J, Aristizabal-Corrales D, Hsu CH, Aravind L, He C,
786 Shi Y. 2015. DNA Methylation on N^{6}-Adenine in *C. elegans*. *Cell* **161**(4): 868-878.

787 Hamilton EP, Kapusta A, Huvos PE, Bidwell SL, Zafar N, Tang H, Hadjithomas M,
788 Krishnakumar V, Badger JH, Caler EV et al. 2016. Structure of the germline genome of
789 *Tetrahymena thermophila* and relationship to the massively rearranged somatic genome.
790 *Elife* **5**.

791 Iyer LM, Abhiman S, Aravind L. 2011. Natural history of eukaryotic DNA methylation systems.
792 *Prog Mol Biol Transl Sci* **101**: 25-104.

793 Iyer LM, Zhang D, Aravind L. 2016. Adenine methylation in eukaryotes: Apprehending the
794 complex evolutionary history and functional potential of an epigenetic modification.
795 *Bioessays* **38**(1): 27-40.

796 Jeltsch A. 2006. On the enzymatic properties of Dnmt1: specificity, processivity, mechanism of
797 linear diffusion and allosteric regulation of the enzyme. *Epigenetics* **1**(2): 63-66.

798 Karrer KM. 2012. Nuclear dualism. *Method Cell Biol* **109**: 29-52.

799 Kong Y, Cao L, Deikus G, Fan Y, Mead EA, Lai W, Zhang Y, Yong R, Sebra R, Wang H et al.
800 2022. Critical assessment of DNA adenine methylation in eukaryotes using quantitative
801 deconvolution. *Science* **375**(6580): 515-522.

802 Koziol MJ, Bradshaw CR, Allen GE, Costa ASH, Frezza C, Gurdon JB. 2016. Identification of
803 methylated deoxyadenosines in vertebrates reveals diversity in DNA modifications. *Nat*
804 *Struct Mol Biol* **23**(1): 24-30.

805 Krietenstein N, Abraham S, Venev SV, Abdennur N, Gibcus J, Hsieh TS, Parsi KM, Yang L,
806 Maehr R, Mirny LA et al. 2020. Ultrastructural details of mammalian chromosome
807 architecture. *Mol Cell* **78**(3): 554-565 e557.

808 Li H, Handsaker B, Wysoker A, Fennell T, Ruan J, Homer N, Marth G, Abecasis G, Durbin R.
809 2009. The sequence alignment/map format and SAMtools. *Bioinformatics* **25**(16): 2078-
810 2079.

811 Liang Z, Shen L, Cui X, Bao S, Geng Y, Yu G, Liang F, Xie S, Lu T, Gu X et al. 2018. DNA N(6)-
812 adenine methylation in *Arabidopsis thaliana*. *Dev Cell* **45**(3): 406-416 e403.

Lister R, Pelizzola M, Dowen RH, Hawkins RD, Hon G, Tonti-Filippini J, Nery JR, Lee L, Ye Z, Ngo Q-M. 2009. Human DNA methylomes at base resolution show widespread epigenomic differences. *Nature* **462**(7271): 315-322.

Liu J, Zhu Y, Luo GZ, Wang X, Yue Y, Wang X, Zong X, Chen K, Yin H, Fu Y et al. 2016. Abundant DNA 6mA methylation during early embryogenesis of zebrafish and pig. *Nat Commun* **7**: 13052.

Liu X, Lai W, Li Y, Chen S, Liu B, Zhang N, Mo J, Lyu C, Zheng J, Du YR et al. 2021a. N(6)-methyladenine is incorporated into mammalian genome by DNA polymerase. *Cell Res* **31**(1): 94-97.

Liu Y, Nan B, Niu J, Kapler GM, Gao S. 2021b. An optimized and versatile counter-flow centrifugal elutriation workflow to obtain synchronized eukaryotic cells. *Front Cell Dev Biol* **9**: 664418.

Luo GZ, Hao Z, Luo L, Shen M, Sparvoli D, Zheng Y, Zhang Z, Weng X, Chen K, Cui Q et al. 2018. N(6)-methyldeoxyadenosine directs nucleosome positioning in *Tetrahymena* DNA. *Genome Biol* **19**(1): 200.

Lyu C, Niu Y, Lai W, Wang Y, Wang Y, Dai P, Ma C, Chen S, Li Y, Jiang G et al. 2022. Rare and misincorporated DNA N(6)-methyladenine is a hallmark of cytotoxic stresses for selectively stimulating the stemness and proliferation of glioblastoma cells. *Cell Discov* **8**(1): 39.

Mondo SJ, Dannebaum RO, Kuo RC, Louie KB, Bewick AJ, LaButti K, Haridas S, Kuo A, Salamov A, Ahrendt SR et al. 2017. Widespread adenine N^6-methylation of active genes in fungi. *Nat Genet* **49**(6): 964-968.

Murray IA, Morgan RD, Luyten Y, Fomenkov A, Correa IR, Jr., Dai N, Allaw MB, Zhang X, Cheng X, Roberts RJ. 2018. The non-specific adenine DNA methyltransferase M.EcoGII. *Nucleic Acids Res* **46**(2): 840-848.

Musheev MU, Baumgartner A, Krebs L, Niehrs C. 2020. The origin of genomic N(6)-methyl-deoxyadenosine in mammalian cells. *Nat Chem Biol* **16**(6): 630-634.

O'Brown ZK, Boulias K, Wang J, Wang SY, O'Brown NM, Hao Z, Shibuya H, Fady PE, Shi Y, He C et al. 2019. Sources of artifact in measurements of 6mA and 4mC abundance in eukaryotic genomic DNA. *BMC Genom* **20**(1): 445.

Quinlan AR, Hall IM. 2010. BEDTools: a flexible suite of utilities for comparing genomic features. *Bioinformatics* **26**(6): 841-842.

Schiffers S, Ebert C, Rahimoff R, Kosmatchev O, Steinbacher J, Bohne AV, Spada F, Michalakis S, Nickelsen J, Muller M et al. 2017. Quantitative LC-MS provides no evidence for m(6)dA or m(4)dC in the genome of mouse embryonic stem cells and tissues. *Angew Chem Int Ed Engl* **56**(37): 11268-11271.

Seabold, Skipper, Perktold J. 2010. Statsmodels: econometric and statistical modeling with Python. *Proc of the 9th Python in Science Conf*.

Sen M, Mooijman D, Chialastri A, Boisset J-C, Popovic M, Heindryckx B, Chuva de Sousa Lopes SM, Dey SS, van Oudenaarden A. 2021. Strand-specific single-cell methylomics reveals distinct modes of DNA demethylation dynamics during early mammalian development. *Nat Commun* **12**(1): 1286.

Sheng Y, Duan L, Cheng T, Qiao Y, Stover NA, Gao S. 2020. The completed macronuclear genome of a model ciliate *Tetrahymena thermophila* and its application in genome scrambling and copy number analyses. *Sci China Life Sci* **63**(10): 1534-1542.

Shipony Z, Marinov GK, Swaffer MP, Sinnott-Armstrong NA, Skotheim JM, Kundaje A, Greenleaf WJ. 2020. Long-range single-molecule mapping of chromatin accessibility in eukaryotes. *Nat Methods* **17**(3): 319-327.

Stergachis AB, Debo BM, Haugen E, Churchman LS, Stamatoyannopoulos JA. 2020. Single-molecule regulatory architectures captured by chromatin fiber sequencing. *Science* **368**(6498): 1449-1454.

Tse OYO, Jiang P, Cheng SH, Peng W, Shang H, Wong J, Chan SL, Poon LCY, Leung TY, Chan KCA et al. 2021. Genome-wide detection of cytosine methylation by single molecule real-time sequencing. *Proc Natl Acad Sci U S A* **118**(5).

Urig S, Gowher H, Hermann A, Beck C, Fatemi M, Humeny A, Jeltsch A. 2002. The *Escherichia coli* dam DNA methyltransferase modifies DNA in a highly processive reaction. *J Mol Biol* **319**(5): 1085-1096.

Vovis GF, Lacks S. 1977. Complementary action of restriction enzymes endo R-*Dpn*I and Endo R-*Dpn*II on bacteriophage f1 DNA. *J Mol Biol* **115**(3): 525-538.

Wang X, Li Z, Zhang Q, Li B, Lu C, Li W, Cheng T, Xia Q, Zhao P. 2018. DNA methylation on N^6-adenine in lepidopteran *Bombyx mori*. *Biochim Biophys Acta Gene Regul Mech* **1861**(9): 815-825.

Wang Y, Chen X, Sheng Y, Liu Y, Gao S. 2017. N^6-adenine DNA methylation is associated with the linker DNA of H2A.Z-containing well-positioned nucleosomes in Pol II-transcribed genes in *Tetrahymena*. *Nucleic Acids Res* **45**(20): 11594-11606.

Wang Y, Sheng Y, Liu Y, Zhang W, Cheng T, Duan L, Pan B, Qiao Y, Liu Y, Gao S. 2019. A distinct class of eukaryotic MT-A70 methyltransferases maintain symmetric DNA N^6-adenine methylation at the ApT dinucleotides as an epigenetic mark associated with transcription. *Nucleic Acids Res* **47**(22): 11771-11789.

Wenger AM, Peluso P, Rowell WJ, Chang PC, Hall RJ, Concepcion GT, Ebler J, Fungtammasan A, Kolesnikov A, Olson ND et al. 2019. Accurate circular consensus long-read sequencing improves variant detection and assembly of a human genome. *Nat Biotechnol* **37**(10): 1155-1162.

Wu TP, Wang T, Seetin MG, Lai Y, Zhu S, Lin K, Liu Y, Byrum SD, Mackintosh SG, Zhong M et al. 2016. DNA methylation on N(6)-adenine in mammalian embryonic stem cells. *Nature* **532**(7599): 329-333.

Xiao CL, Zhu S, He M, Chen, Zhang Q, Chen Y, Yu G, Liu J, Xie SQ, Luo F et al. 2018. N(6)-methyladenine DNA modification in the human genome. *Mol Cell* **71**(2): 306-318 e307.

Xiong J, Gao S, Dui W, Yang W, Chen X, Taverna SD, Pearlman RE, Ashlock W, Miao W, Liu Y. 2016. Dissecting relative contributions of cis- and trans-determinants to nucleosome distribution by comparing Tetrahymena macronuclear and micronuclear chromatin. *Nucleic Acids Res* **44**(21): 10091-10105.

Yan J, Liu F, Guan Z, Yan X, Jin X, Wang Q, Wang Z, Yan J, Zhang D, Liu Z et al. 2023. Structural insights into DNA N^6-adenine methylation by the MTA1 complex. *Cell Discov* **9**(1): 8.

Zhang G, Huang H, Liu D, Cheng Y, Liu X, Zhang W, Yin R, Zhang D, Zhang P, Liu J et al. 2015. N^6-methyladenine DNA modification in *Drosophila*. *Cell* **161**(4): 893-906.

Zhou C, Wang C, Liu H, Zhou Q, Liu Q, Guo Y, Peng T, Song J, Zhang J, Chen L et al. 2018. Identification and analysis of adenine N(6)-methylation sites in the rice genome. *Nat Plants* **4**(8): 554-563.

Figure Legends

Figure 1. Exclusive methylation at the ApT dinucleotide in *Tetrahymena*. **A.** Overview of 6mA detection by SMRT sequencing. **B.** A schematic diagram for SMRT CCS. **C.** IPD ratios (IPDr) for all A sites in a typical SMRT CCS read mapped to the *Tetrahymena* MAC reference genome. The IPDr threshold was set at 2.38, separating 6mA from unmodified A. Note the localization of 6mA clusters in linker DNA between the canonical nucleosome array within the gene body. **D.** IPDr distributions (log_2) of all A sites in WT (top) and Δ*AMT1* cells (bottom). Also plotted were distributions for A sites at the ApA, ApC, ApG, and ApT dinucleotide, respectively. **E.** Deconvolution of the 6mA peak and the unmodified A peak for IPDr distributions (log_2) at the ApT dinucleotide. Note the low false positive and false negative rates of 6mA calling in WT (top) and Δ*AMT1* cells (bottom).

Figure 2. Distinguishing hemi- and full-6mApT. **A.** Four states of ApT duplexes: full methylation, hemi-W, hemi-C, and unmethylated, distinguished by IPDr of adenine sites on W and C, respectively. **B.** Distribution of ApT duplexes according to IPDr of adenine sites on W and C, respectively. Note the abundance of the full methylation state in WT and its absence in Δ*AMT1* cells. **C.** Demarcation of the four methylation states of ApT duplexes in WT (left) and Δ*AMT1* cells (right) by their IPDr on W and C, respectively. Left: For bulk ApT duplexes, the IPDr threshold for 6mA calling was set at 2.38, according to deconvolution based on Gaussian fitting of the small 6mA peak. For ApT duplexes with one 6mA as defined above, the IPDr threshold for calling 6mA on the opposite strand was set at 1.57, according to deconvolution based on Gaussian fitting of the small unmodified A peak. Right: For bulk ApT duplexes, the IPDr threshold for 6mA calling was set at 2.55, according to deconvolution based on Gaussian fitting of the small 6mA peak. For ApT duplexes with one 6mA as defined above, the IPDr threshold for calling 6mA on the opposite strand was also set at 2.55, according to

deconvolution based on Gaussian fitting of the small 6mA peak. **D.** Typical DNA molecules from *Tetrahymena* WT (top) and Δ*AMT1* cells (bottom). Note ApT duplexes with distinct methylation states (colored dot) distributed along individual DNA molecules (gray line). A DNA molecule with strong segregation strand bias in WT cells and a genomic position with strong penetrance strand bias in Δ*AMT1* cells were marked.

Figure 3. SMRT CCS detection of BrdU incorporation into newly synthesized DNA. **A.** *In vitro* BrdU-labeling. Specific labeling of either strand (W-labeled or C-labeled) was achieved by primer extension, while labeling of both strands (W&C-labeled) was achieved by PCR. A plasmid fragment containing three fully methylated GATC sites (6mA) was used as the template, as well as the unlabeled control for SMRT CCS. **B.** IPDr distributions ($\log_2$) of all T sites from: both strands in unlabeled and W&C-labeled DNA (50% or 90% BrdUTP; top); only W in unlabeled, W-labeled, and C-labeled DNA (middle); only C in unlabeled, W-labeled, and C-labeled DNA (bottom). IPDr threshold was set at 2.5 for separating BrdU from T. **C.** IPDr for all T (left) or A sites (right) in typical SMRT CCS reads for unlabeled, W-labeled, C-labeled, and W&C-labeled DNA (90% BrdUTP). IPDr thresholds were set at 2.5 for separating BrdU from T, and at 2.7 for separating 6mA from A. **D.** Percentage of $BrdU^+$ molecules in unlabeled, W-labeled, C-labeled, and W&C-labeled DNA (50% and 90% BrdUTP, respectively). $BrdU^+$ molecules were defined as DNA molecules with no less than 8 BrdU sites on one strand (W||C ≥ 8). **E.** Segregation strand biases of BrdU sites in $BrdU^+$ molecules. Segregation strand bias for BrdU was defined as the difference-sum ratio between BrdU sites on W and C: $(\frac{W-C}{W+C})_S$.

Figure 4. Segregation of hemi-6mApT to the parental strand after DNA replication. **A.** $Hemi^+$ molecules are enriched in S phase. *Tetrahymena* cells were synchronized at G1 phase

by centrifugal elutriation and released for growth in the fresh medium (Liu et al. 2021b). Four time points were taken (0, 1.5, 2, and 4h after release) for SMRT CCS. Hemi$^+$ molecules were defined as DNA molecules with a total count of no less than 11 hemi sites (W+C ≥ 11) or with no less than 11 hemi sites on one strand (W||C ≥ 11). The count of hemi$^+$ molecules was normalized first against the counts of total DNA molecules and then against the 0h (G1 phase) value. **B.** Hemi-6mApT sites in hemi$^+$ molecules exhibit strong segregation strand bias. Segregation strand bias for hemi-6mApT is defined as the difference-sum ratio between hemi-W and hemi-C: $(\frac{W-C}{W+C})_S$. **C.** Typical DNA molecules with hemi-6mApT fully segregated to W or C, corresponding to segregation strand bias of +1 and -1, as marked in Fig. 4B. **D.** IPDr distributions of T sites in genomic DNA samples of synchronized *Tetrahymena* cells with BrdU-labeling (1.5h, 2h, and 4h) or without (0h). The IPDr threshold for calling BrdU was set at 2.8. **E.** BrdU sites in BrdU$^+$ molecules exhibit strong segregation strand biases. BrdU$^+$ molecules were defined as DNA molecules with a total count of no less than 15 BrdU sites (W+C ≥ 15). Segregation strand bias for BrdU was defined as the difference-sum ratio between BrdU sites on W and C: $(\frac{W-C}{W+C})_S$. Also shown are typical BrdU$^+$ molecules with BrdU fully segregated to W or C, corresponding to segregation strand bias of +1 and -1, respectively. **F.** Correlation between BrdU-labeling and BrdU$^+$ molecules. BrdU$^+$ molecules were alternatively defined as DNA molecules with a total count of no less than 15 BrdU sites (W+C ≥ 15), or with no less than 15 BrdU sites on one strand (W||C ≥ 15). The latter is more selective for DNA molecules with strong strand segregation bias. **G.** Hemi-6mApT and BrdU are segregated to opposite strands of the DNA duplex. Distribution of hemi$^+$/BrdU$^+$ molecules (hemi-6mApT: W||C ≥ 11; BrdU: W||C ≥ 15) according to their segregation strand bias for hemi-6mApT and BrdU, respectively. **H.** Typical hemi$^+$/BrdU$^+$ molecules with hemi-6mApT and BrdU fully segregated to opposite strands, corresponding to segregation strand bias of (-1, +1) and (+1, -1), as marked in Fig. 4G.

Figure 5. *In vitro* methyltransferase activity of AMT1 complex. **A.** SDS-PAGE of *in vitro* reconstituted AMT1 complex comprising AMT1, AMT7, AMTP1 (1-240 aa), and AMTP2. **B.** The steady-state kinetics of AMT1 complex on a hemi-methylated substrate (hemi), determined by a ^{3}H-SAM based methyltransferase assay. The substrate contains a single ApT duplex (underlined), which is hemi-methylated (red). **C.** Methylation of the unmodified (un) and hemi-methylated (hemi) substrates. Both contain two ApT duplexes (underlined), which are either unmodified or hemi-methylated (red). **D.** IPDr distributions for total adenine, adenine at the ApT dinucleotide, and adenine in ApC dinucleotide, after *in vitro* methylation of human chromatin by either AMT1 complex (top) or M.EcoGII (bottom). **E.** 6mA distribution at all four ApN dinucleotides, after *in vitro* methylation of human chromatin by either AMT1 complex or M.EcoGII. ApN frequencies in SMRT CCS reads are also plotted for comparison (Sequence Average). **F.** Demarcation of the four methylation states of ApT duplexes by their IPDr on W and C, in human chromatin methylated by AMT1 complex (top) or M.EcoGII (bottom). AMT1 complex methylation pattern is reminiscent of that in WT *Tetrahymena* cells, with strong preference for full-6mApT, as indicated by a shift in the IPDr threshold for calling full-6mApT relative to calling bulk 6mA. M.EcoGII methylation pattern is reminiscent of that in Δ*AMT1* cells, with no preference for full-6mApT, as indicated by the same IPDr threshold for calling bulk 6mA or full-6mApT. **G.** Relative abundance of hemi-6mApT and full-6mApT in human chromatin methylated by either AMT1 complex or M.EcoGII. **H.** Model: AMT1-depenent semi-conservative transmission of 6mA.

Figure 6. Chromatin-guided 6mA transmission. **A.** 6mA and nucleosome distributions in *Tetrahymena*. A typical genomic region is shown with SMRT CCS reads mapped across it, as well as annotations of genes and canonical nucleosome arrays (Xiong et al. 2016). Note that 6mApT sites (in either full or hemi-methylation, red dot) distributed along individual DNA

molecules (gray line) are clustered in linker DNA (LD). LD1 is between the +1 and +2 nucleosome (the first and second nucleosome downstream of TSS); LD2 and beyond are defined iteratively further downstream of the gene body. **B.** Periodic 6mA distribution at the single molecule level in *Tetrahymena*. Autocorrelation between 6mA sites (distance ≤ 1 kb) was calculated for individual DNA molecules, ranked by their median absolute deviations, and plotted as a heat map (bottom) and an aggregated correlogram (top). **C.** Autocorrelation of 6mA and nucleosome distributions at the ensemble level in *Tetrahymena* (top), revealing a ~200bp periodicity. Cross-correlation between 6mA and nucleosome distributions (bottom), revealing a ~100bp phase difference between them. **D.** Typical DNA molecules from human chromatin, after *in vitro* methylation by AMT1 complex and M.EcoGII, respectively. Note clusters of 6mA sites (red dot) distributed at regular intervals along individual DNA molecules (gray line). The difference in 6mA density is mostly due to much lower density of the ApT dinucleotide that is preferred by AMT1 complex, relative to essentially all A sites that can be targeted by M.EcoGII. Additionally, AMT1 complex may also have reduced chromatin accessibility relative to M.EcoGII, due to its much larger size. **E.** Periodic 6mA distributions at the single molecule level, after *in vitro* methylation by AMT1 complex and M.EcoGII, respectively. Autocorrelation between 6mA sites (distance ≤ 1kb) was calculated for individual DNA molecules, ranked by their median absolute deviations, and plotted as heat maps (bottom) and aggregated correlograms (top). DNA molecules with regularly spaced 6mA clusters were found across euchromatic and heterochromatic regions. Heterochromatin is known to have low nucleosome positioning, which means at the ensemble level, nucleosomes can occupy alternative genomic positions. However, at the single molecule level, nucleosomes are still regularly spaced, which is only obvious in long-read, single molecule sequencing results. **F.** Congregation of full-6mApT in DNA molecules undergoing hemi-to-full conversion. Their max inter-full distances were often very small, thus rarely represented (probability ≤ 0.01) in simulations with permutated full and hemi positions (box); x- axis: the probability for simulated max inter-full distances to be no greater

than the observed value; y-axis: the count of DNA molecules with the corresponding probability. **G.** Distribution of max inter-full distances for DNA molecules with strong full-6mApT congregation (probability ≤ 0.01, Fig. 5F box). Note the two peaks corresponding to DNA molecules with full-6mApT congregation within a LD (Fig. 5H) and across adjacent LDs (Fig. 5I), respectively. **H.** Full-6mApT congregation within a LD. **I.** Full-6mApT congregation across adjacent LDs.

Figure 7. AMT1-independent *de novo* methylation. **A.** Depletion of high penetrance 6mA positions in Δ*AMT1* relative to WT cells. **B.** Strong 6mA segregation strand biases in Δ*AMT1* cells. Chi-squared analysis was performed on DNA molecules with the specified number of total 6mA (full-6mApT counted as two, hemi-6mApT counted as one; x-axis), the percentage of DNA molecules with strong bias for 6mA segregation to one strand was indicated (expectance < 5%, assuming random distribution; y-axis). WT cells were also analyzed as a negative control. **C.** Increased 6mA variability at the gene level in Δ*AMT1* relative to WT cells. For each gene, we calculated the coefficients of variance (CV) of 6mA counts from individual DNA molecules fully covering the gene, for WT and Δ*AMT1* cells, respectively. We then plotted the distribution of the ratio between the two CV values ($\frac{WT}{\Delta AMT1}$) across all genes. Note that for most genes, the ratio is less than 1 (i.e., 6mA variability is higher in Δ*AMT1* than WT cells). **D.** Penetrance strand bias of 6mA in WT and Δ*AMT1* cells. 6mA penetrance strand bias is defined for an ApT position in the genome as the difference-sum ratio between the number of DNA molecules supporting 6mA on W and C, respectively: $(\frac{W-C}{W+C})_{\mathrm{p}}$. We plotted the distribution of ApT genomic positions according to their penetrance strand bias (top). We also plotted their distribution according to both penetrance strand bias and 6mApT coverage (middle: WT; bottom: Δ*AMT1*). In WT cells, most ApT positions had penetrance strand bias values around 0 (i.e., similar

numbers of 6mA on W and C), while few had values at +1 (6mA only on W) or -1 (6mA only on C). The latter most likely corresponds to genomic positions exclusive for AMT1-indpendent methylation (Fig 6F: left panel). The opposite was true for Δ*AMT1* cells. **E.** Representative genomic positions in *Tetrahymena* rDNA (top schematic: only the left half of the palindromic dimer, from telomere to dyad, is shown) targeted by AMT1-indpendent (left) and AMT1-dependent methylation (right). Note that 6mA occurs only on one strand in AMT1-independent methylation, but on both strands in AMT1-depedendent methylation. **F.** 6mA penetrance of individual genomic positions in WT and Δ*AMT1* cells. Note the two distinct groups corresponding to (1) AMT1-indpendent and (2) AMT1-dependent methylation. **G.** 10-bp cycle of 6mA penetrance strand bias in Δ*AMT1* cells (top left), suggesting that the dedicated *de novo* 6mA-MTase can only approach the DNA substrate from one side (top right). Lack of such pattern in WT cells (bottom left) supports that AMT1 complex can approach from different sides (bottom right). **H.** Overlap in ApT positions methylated in WT or Δ*AMT1* cells (6mA penetrance ≥ 0.1). **I.** 6mA levels of individual genes in WT and Δ*AMT1* cells are strongly correlated. Each gene is assigned a coordinate: sum of 6mA penetrance values for all methylated ApT positions in the gene body (ΣP) for WT (x-axis) and Δ*AMT1* cells (y-axis). The Spearman's rank correlation coefficient is significant ($p < 0.01$**).

Figure 8. Comparison of 6mA and 5mC pathways in eukaryotes. See text for details.

Table

Table 1. 6mA statistics in WT and Δ*AMT1* cells. **Top:** the number of total ApT (with or without modification) and 6mApT sites in DNA molecules fully mapped to the MAC. Both W and C are counted. Percentage of DNA methylation is also calculated ($\frac{6mApT}{total\ ApT}$). **Bottom:** the number of full-6mApT and hemi-6mApT duplexes. Note that each full-6mApT duplex contains two 6mA sites, while each hemi-6mApT duplex only contains one site. Percentages of full-6mApT and hemi-6mApT duplexes are also calculated.

Single molecule	WT		Δ*AMT1*	
	Number	Percentage (%)	Number	Percentage (%)
ApT	992,618,784	100	842,024,326	100
6mApT sites	18,750,787	1.89	4,248,723	0.50
Full	8,373,723	89.32	64,270	3.03
Hemi-W	998,137	5.32	2,051,797	48.29
Hemi-C	1,005,304	5.36	2,068,386	48.68
Total 6mApT	18,750,787	100	4,248,723	100

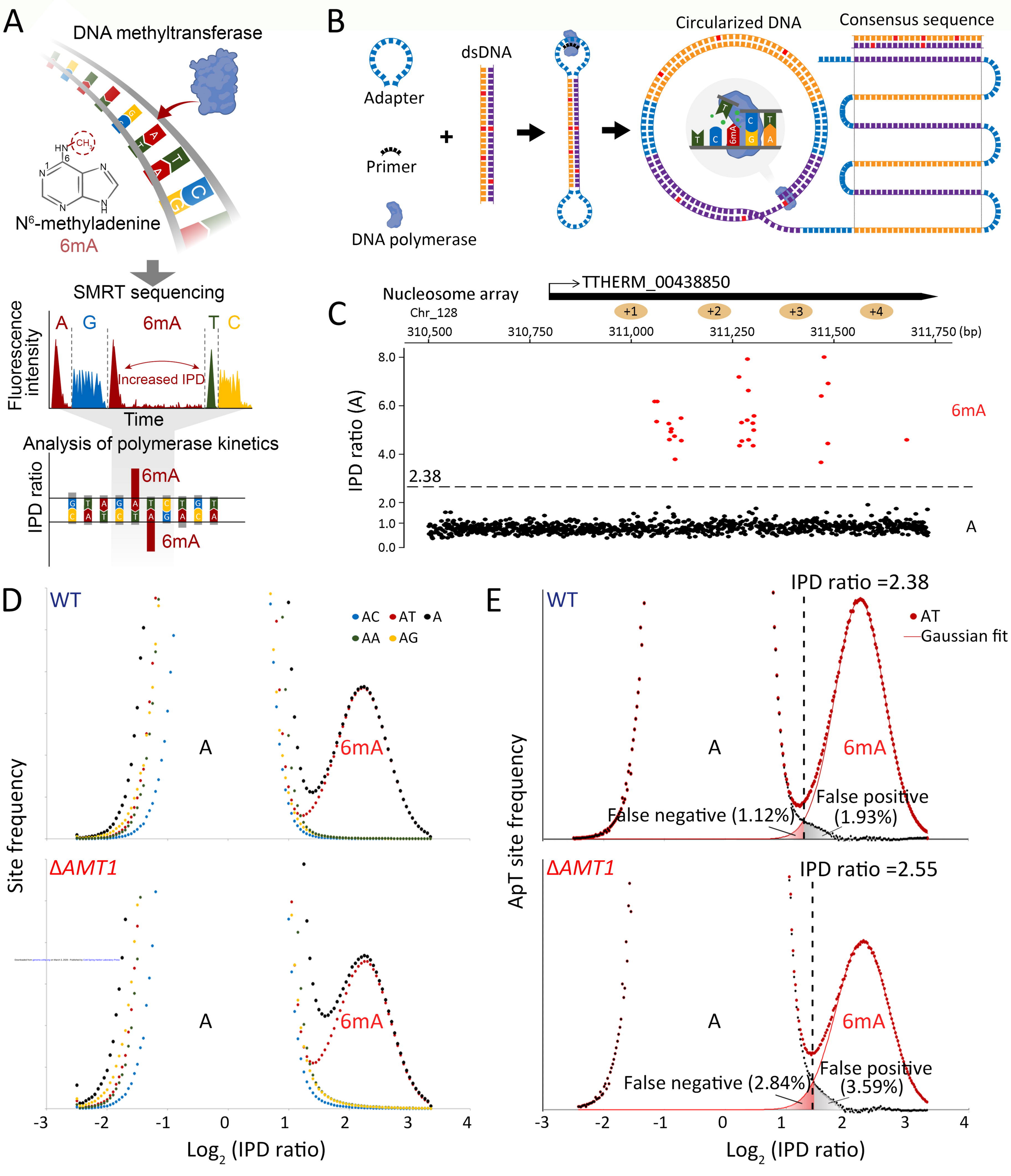

A

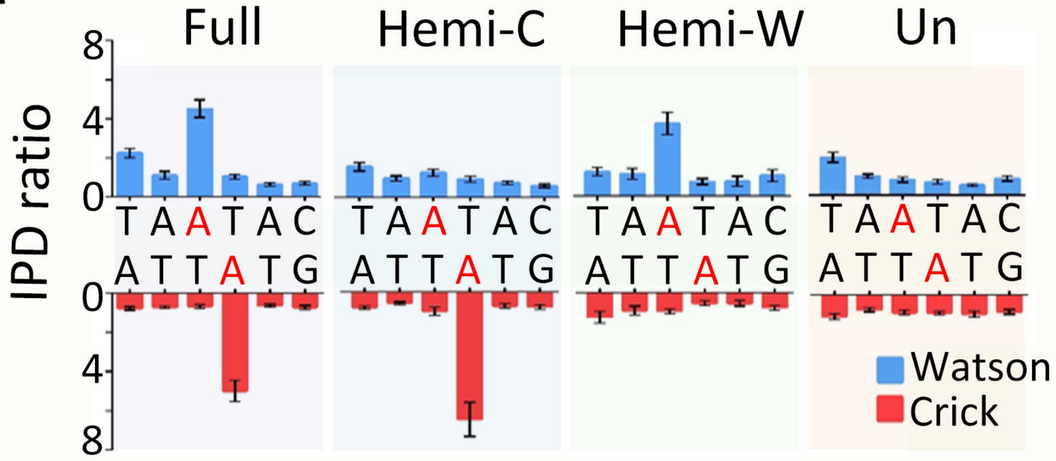

B

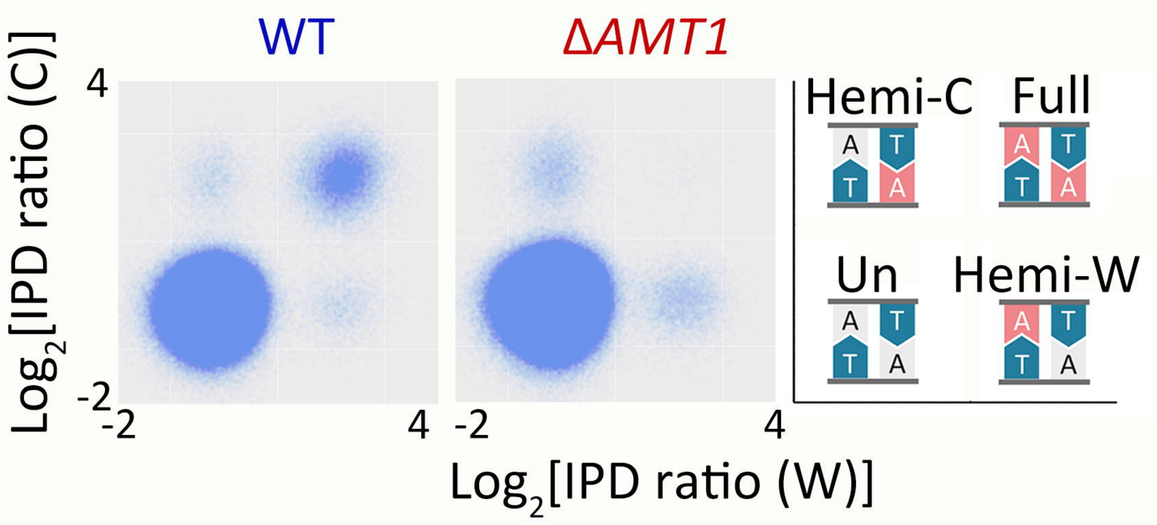

C

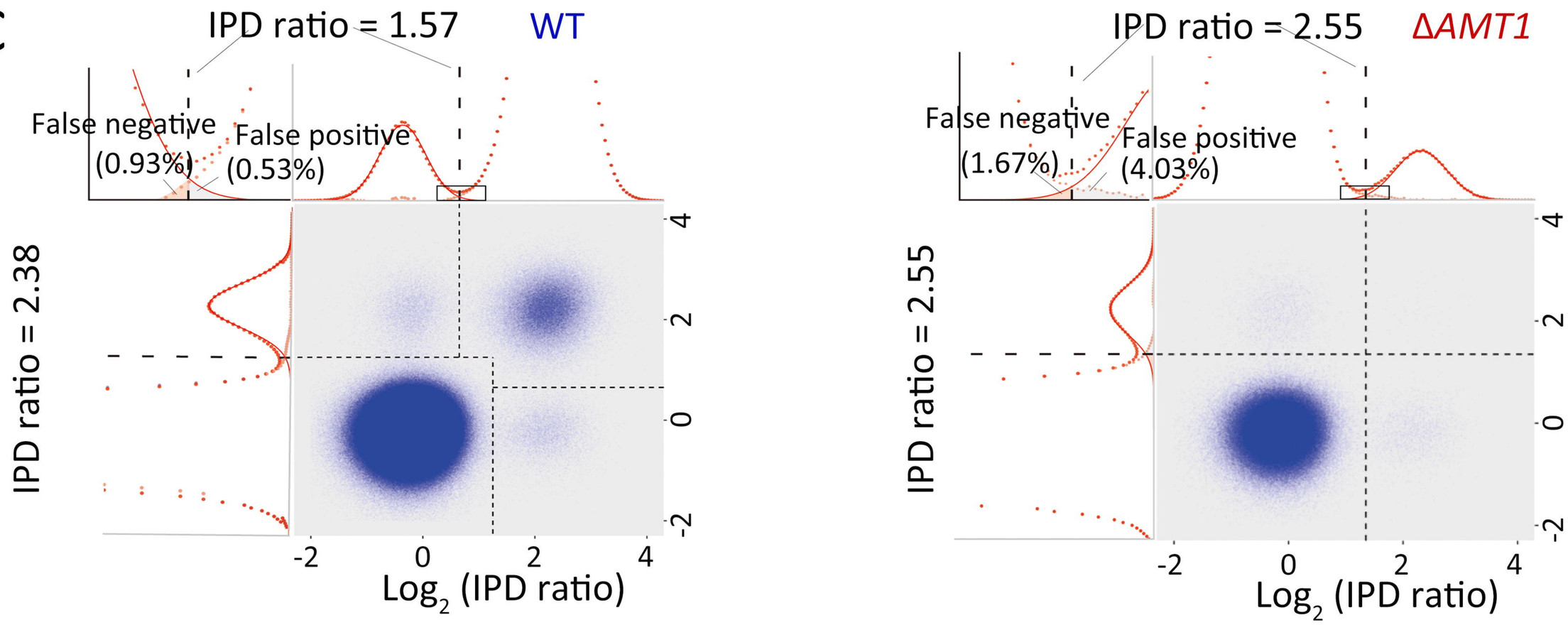

D

A

In vitro BrdU-labeling

Unlabeled

PCR

W&C-labeled

W-labeled

Primer extension

C-labeled

Full methylation (GATC)

Hemi-C

Hemi-W

No methylation

Newly synthesized DNA (BrdU-labeled)

B

IPD ratio = 2.5

W&C

Unlabeled

50% BrdUTP PCR

90% BrdUTP PCR

W

Unlabeled

C-labeled

W-labeled

C

Unlabeled

W-labeled

C-labeled

Percentage (%)

0.1

0.05

0

-3

-2

0

2

4

Log_2 (IPD ratio)

C

T

A

W-strand

C-strand

Unlabeled

W-labeled

C-labeled

W&C-labeled

IPD ratio

6

2.5

8

2.7

250

500

750

1000 (bp)

D

$BrdU^+$

$BrdU^+$ percentage (%)

20

15

12.04

10

5

0.5

3.68

1.09

14.13

0.1

0.075

0.05

0.025

0

0.01

Unlabeled

W-labeled

C-labeled

W&C-labeled (50%)

W&C-labeled (90%)

E

BrdU segregation strand bias

C- labeled

W-labeled

Percentage (%)

80

60

40

20

0

-1

-0.5

0

0.5

1

BrdU $(\frac{W-C}{W+C})_S$

A

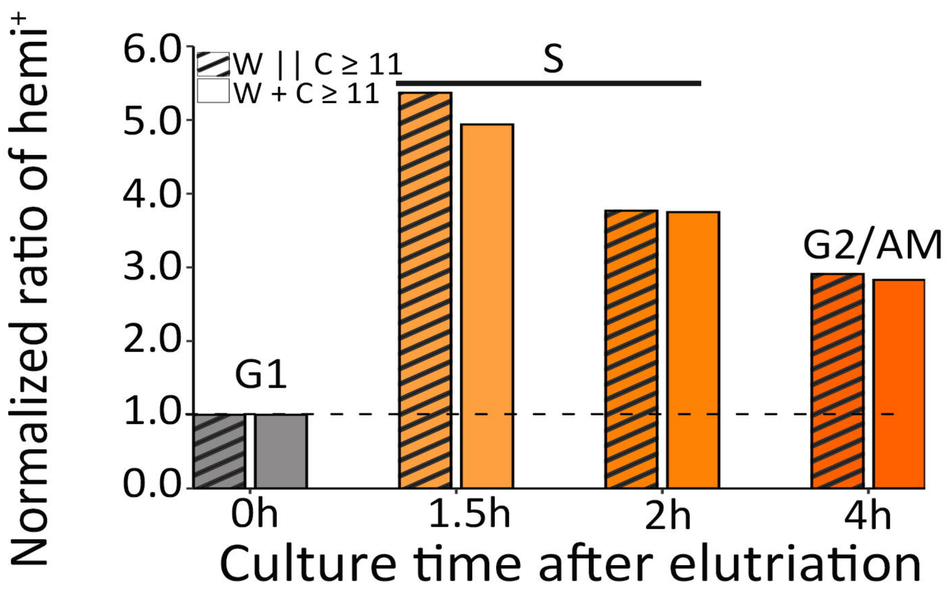
Normalized ratio of hemi+
W || C ≥ 11
W + C ≥ 11
S
G1
G2/AM
6.0
5.0
4.0
3.0
2.0
1.0
0.0
0h
1.5h
2h
4h
Culture time after elutriation

B

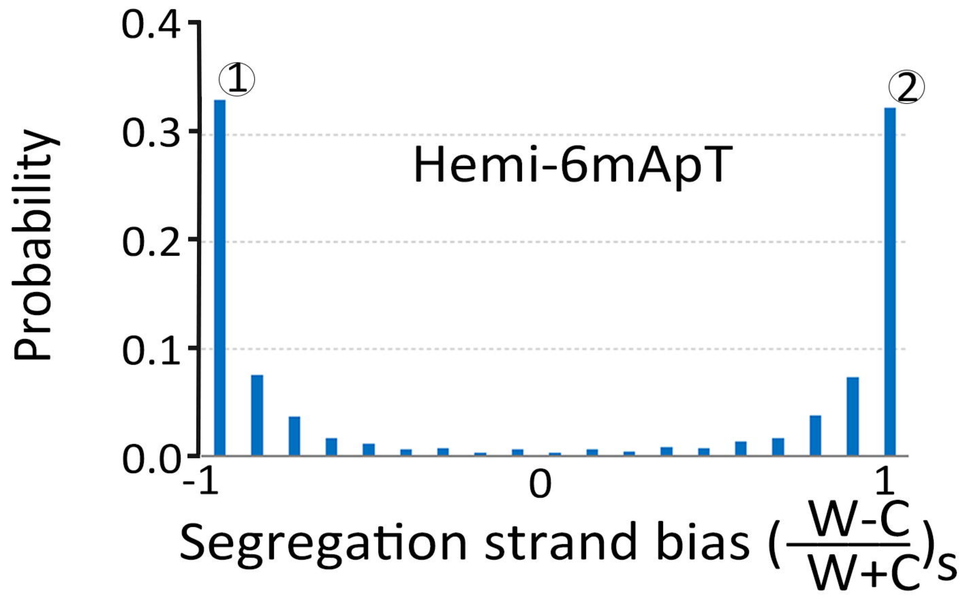
Probability
Hemi-6mApT
①
②
0.4
0.3
0.2
0.1
0.0
-1
0
1
Segregation strand bias (W-C / W+C)s

C

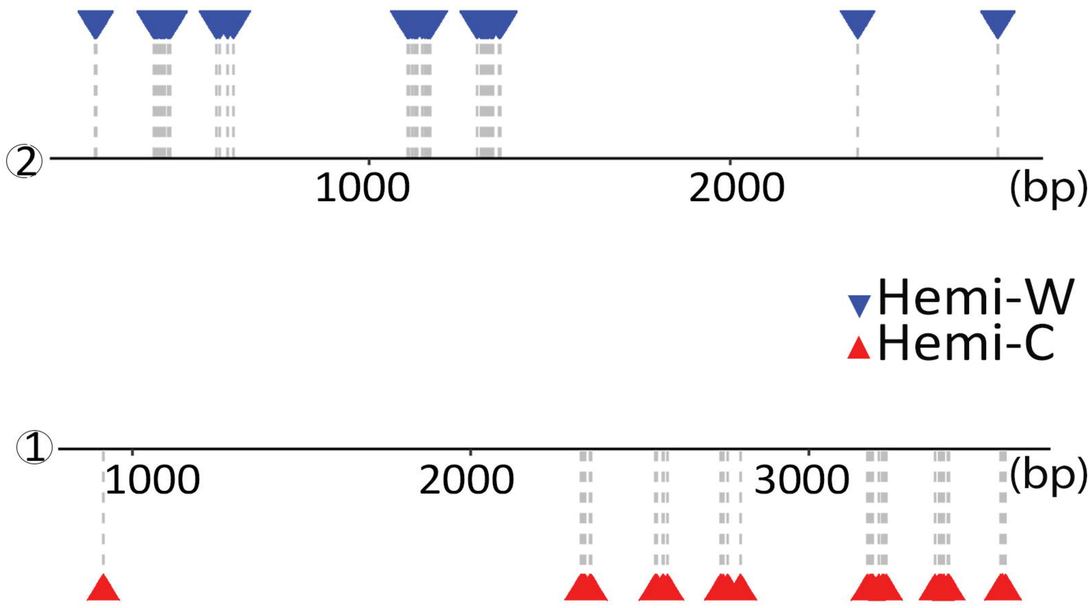
②
1000
2000
(bp)
Hemi-W
Hemi-C
①
1000
2000
3000
(bp)

D

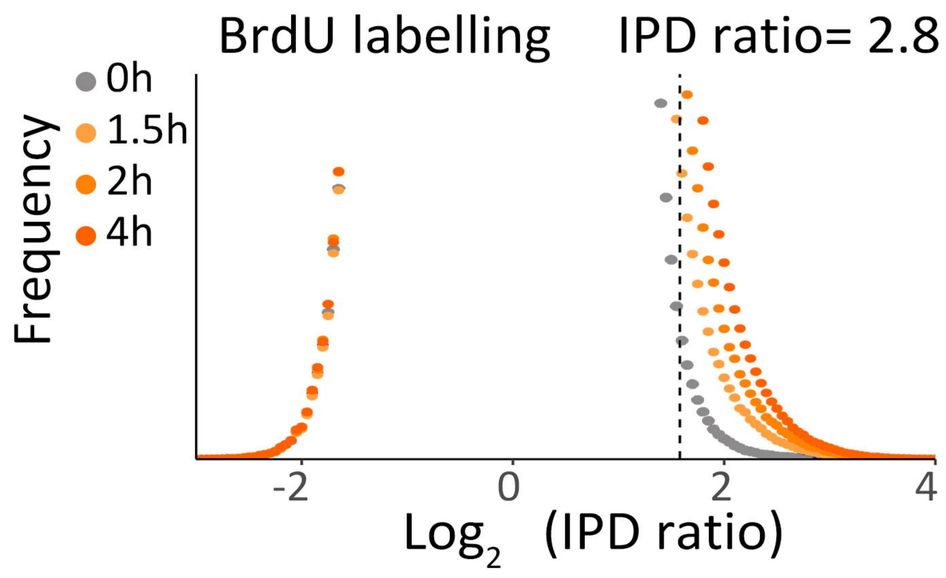
BrdU labelling
IPD ratio= 2.8
Frequency
0h
1.5h
2h
4h
-2
0
2
4
Log2 (IPD ratio)

E

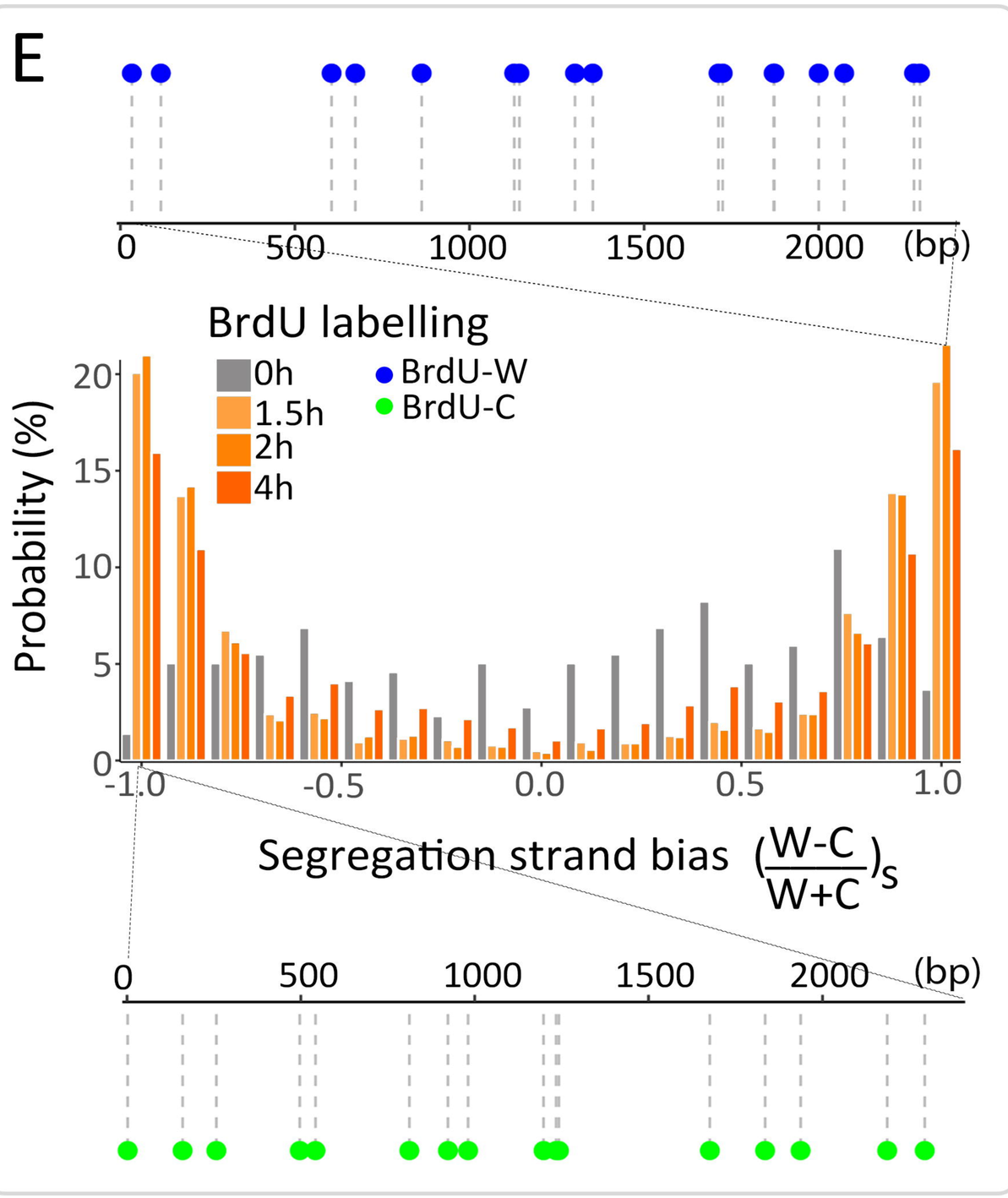
0
500
1000
1500
2000
(bp)
BrdU labelling
0h
1.5h
2h
4h
BrdU-W
BrdU-C
Probability (%)
20
15
10
5
0
-1.0
-0.5
0.0
0.5
1.0
Segregation strand bias (W-C / W+C)s
0
500
1000
1500
2000
(bp)

F

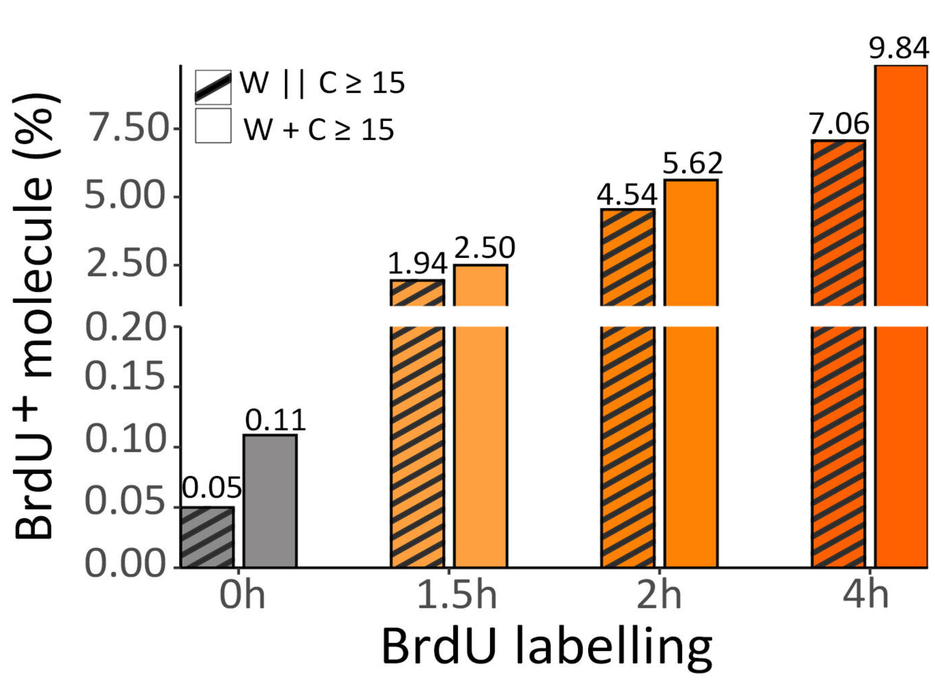
W || C ≥ 15
W + C ≥ 15
BrdU+ molecule (%)
7.50
5.00
2.50
0.20
0.15
0.10
0.05
0.00
0.05
0.11
1.94
2.50
4.54
5.62
7.06
9.84
0h
1.5h
2h
4h

G

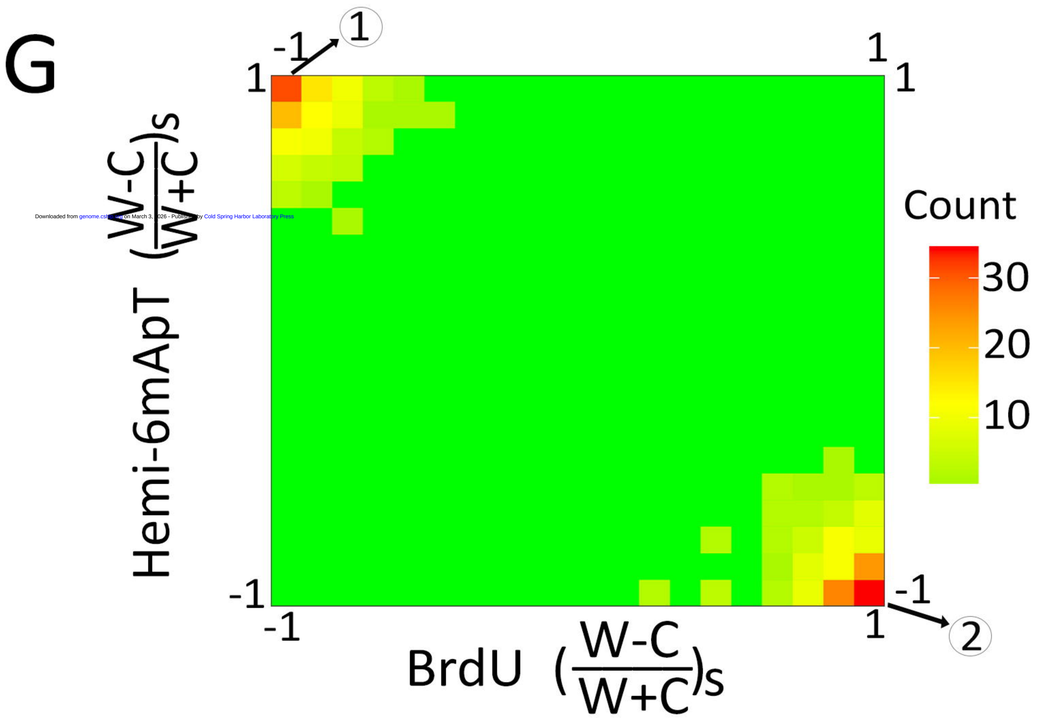
BrdU labelling
Hemi-6mApT (W-C / W+C)s
BrdU (W-C / W+C)s
-1
1
Count
30
20
10
①
②

H

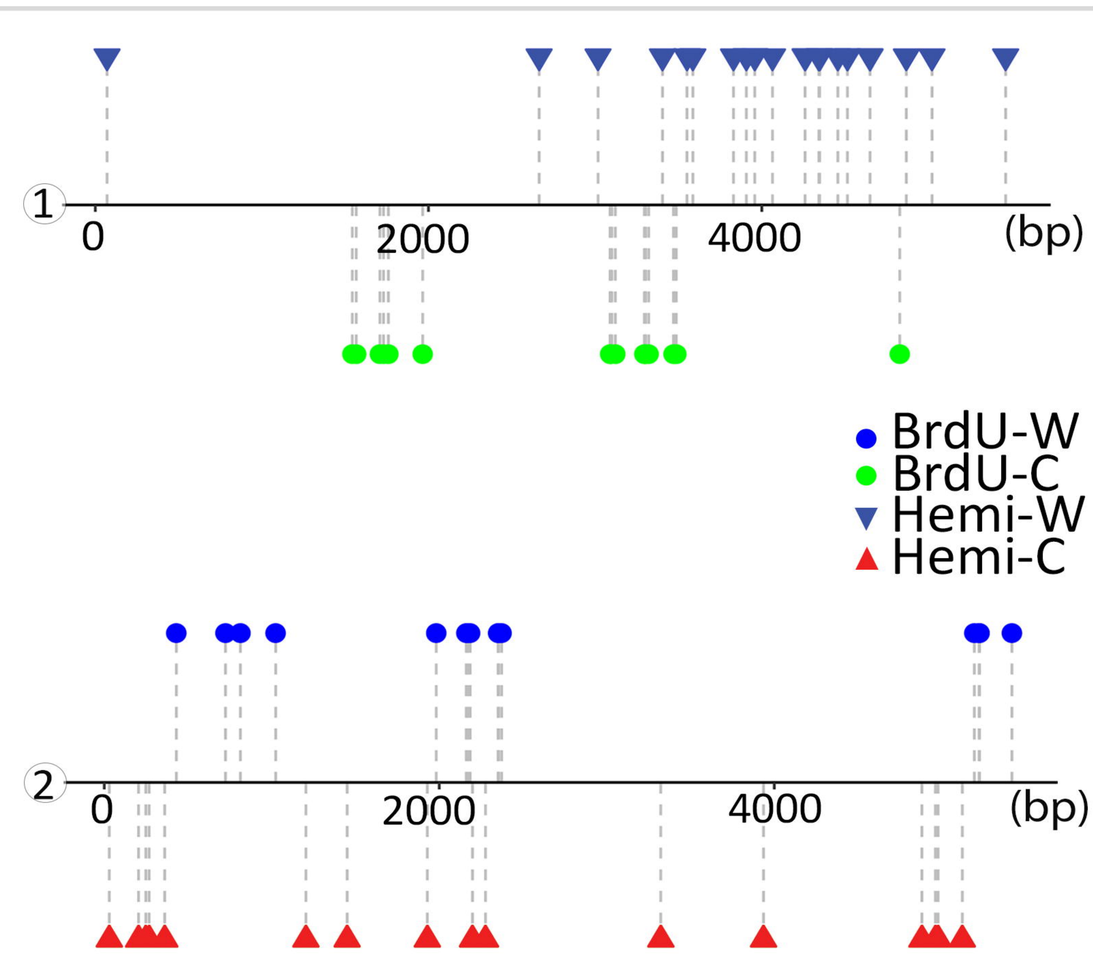
①
0
2000
4000
(bp)
BrdU-W
BrdU-C
Hemi-W
Hemi-C
②
0
2000
4000
(bp)

A

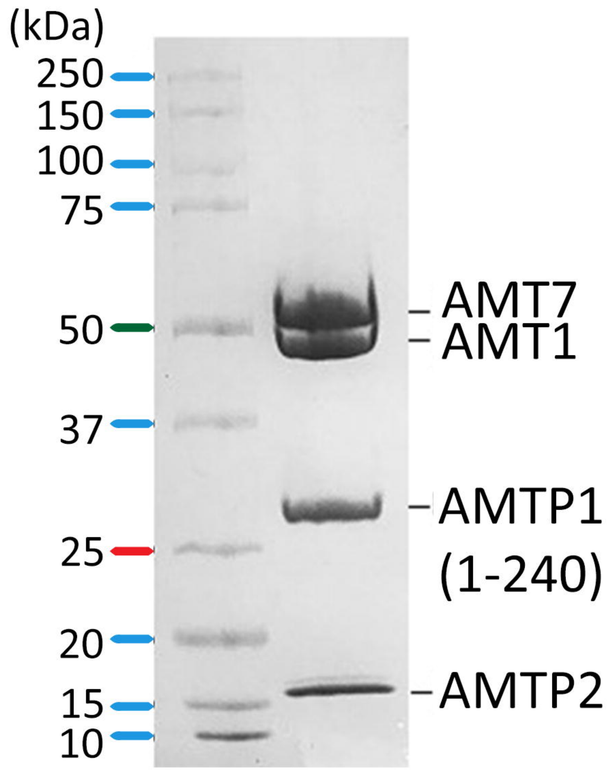
(kDa)
250
150
100
75
50
37
25
20
15
10
AMT7
AMT1
AMTP1
(1-240)
AMTP2

B

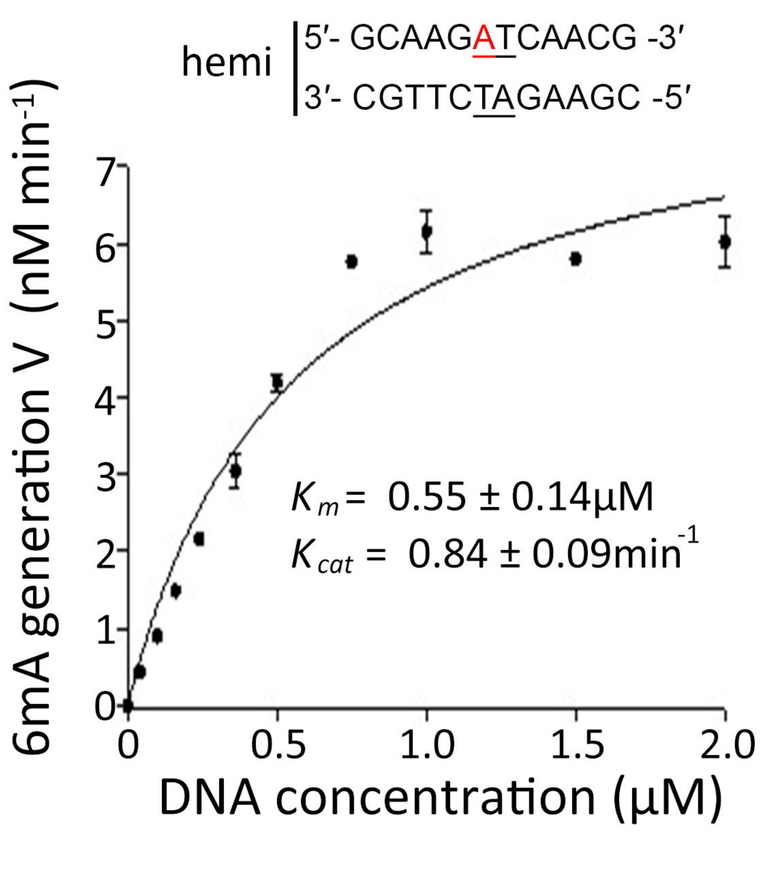
hemi
5′- GCAAGATCAACG -3′
3′- CGTTCTAGAAGC -5′
6mA generation V (nM min-1)
K_m = 0.55 ± 0.14μM
K_{cat} = 0.84 ± 0.09min-1
DNA concentration (μM)

C

un
5′- AACTTCTGTCATTACATTAAGCTTTAA -3′
3′- TTGAAGACAGTAATGTAATTCGAAATT -5′
hemi
5′- AACTTCTGTCATTACATTAAGCTTTAA -3′
3′- TTGAAGACAGTAATGTAATTCGAAATT -5′
counts per minute (× 10³)
un
hemi

D

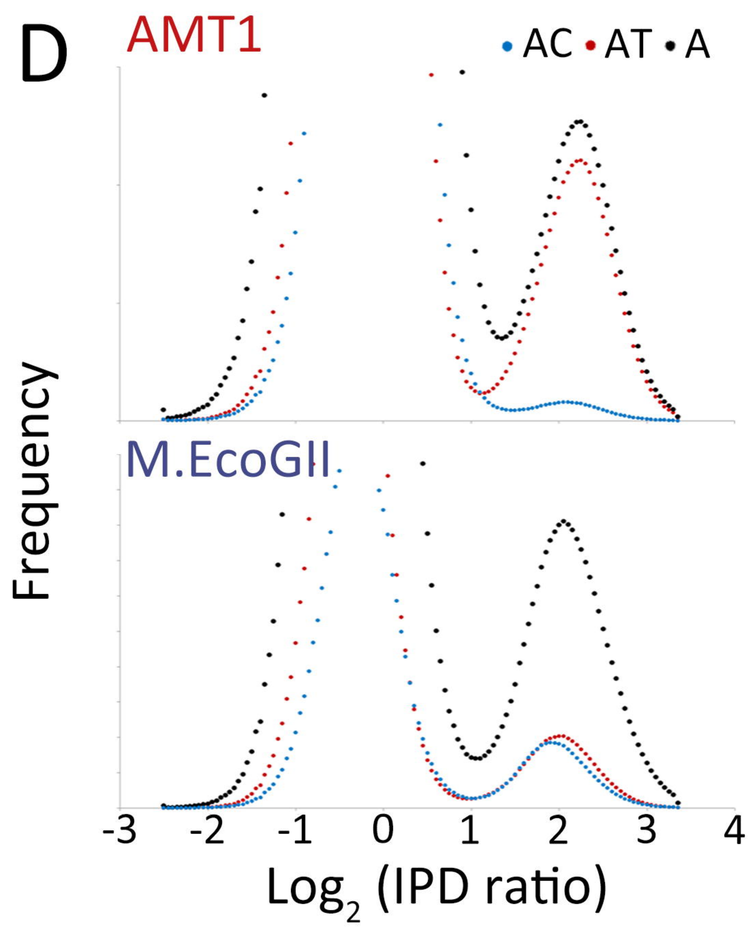
AMT1
AC
AT
A
M.EcoGII
Frequency
Log2 (IPD ratio)

F

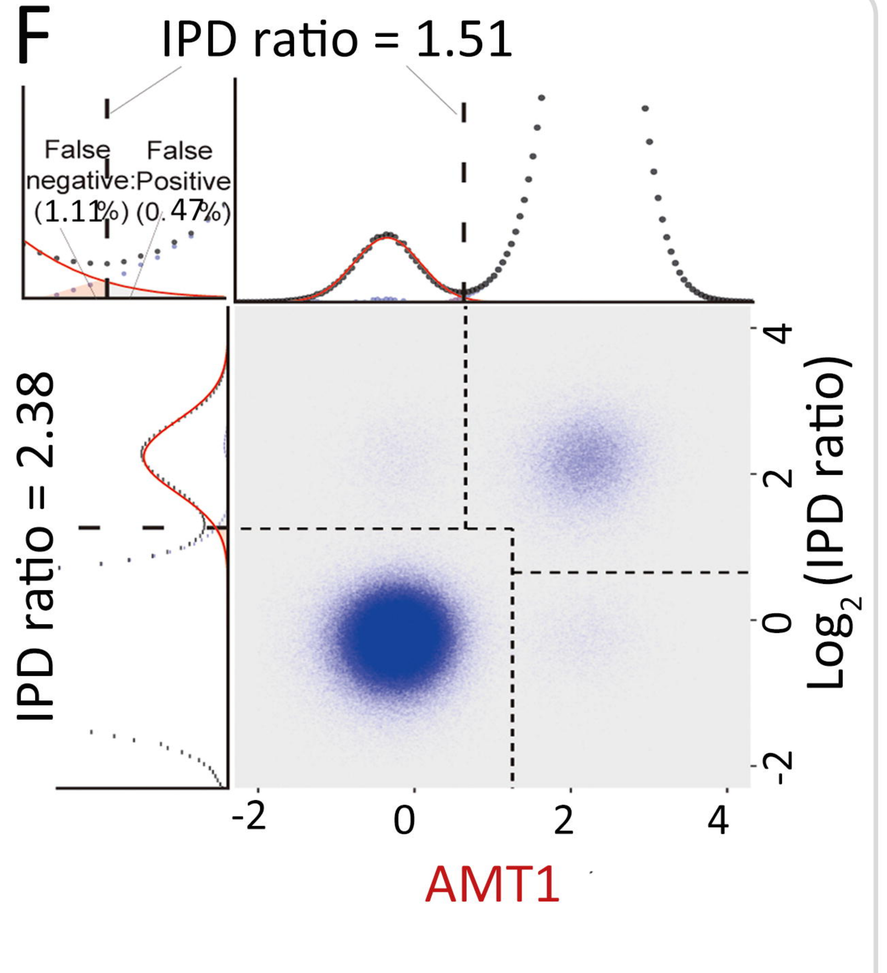
IPD ratio = 1.51
False negative (1.11%)
False Positive (0.47%)
IPD ratio = 2.38
Log2 (IPD ratio)
AMT1
IPD ratio = 2.00
False negative (0.69%)
False Positive (1.74%)
IPD ratio = 2.00
Log2 (IPD ratio)
M.EcoGII

E

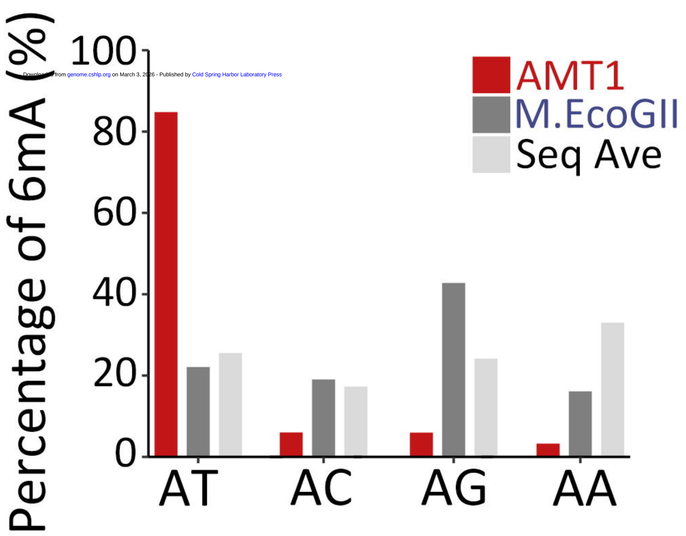
Percentage of 6mA (%)
AMT1
M.EcoGII
Seq Ave
AT
AC
AG
AA

G

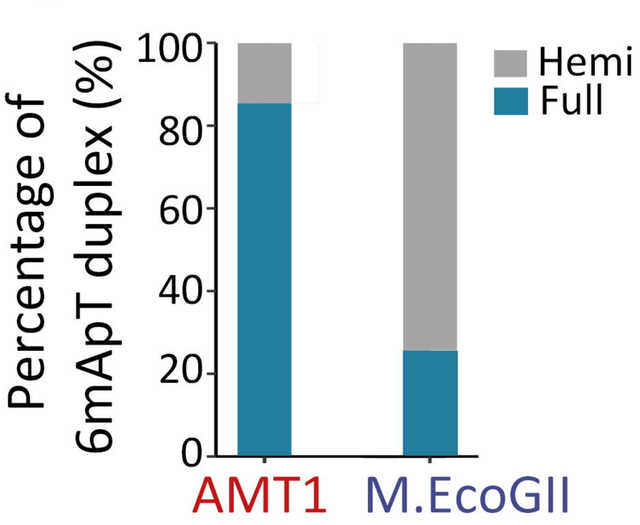
Percentage of 6mApT duplex (%)
Hemi
Full
AMT1
M.EcoGII

H

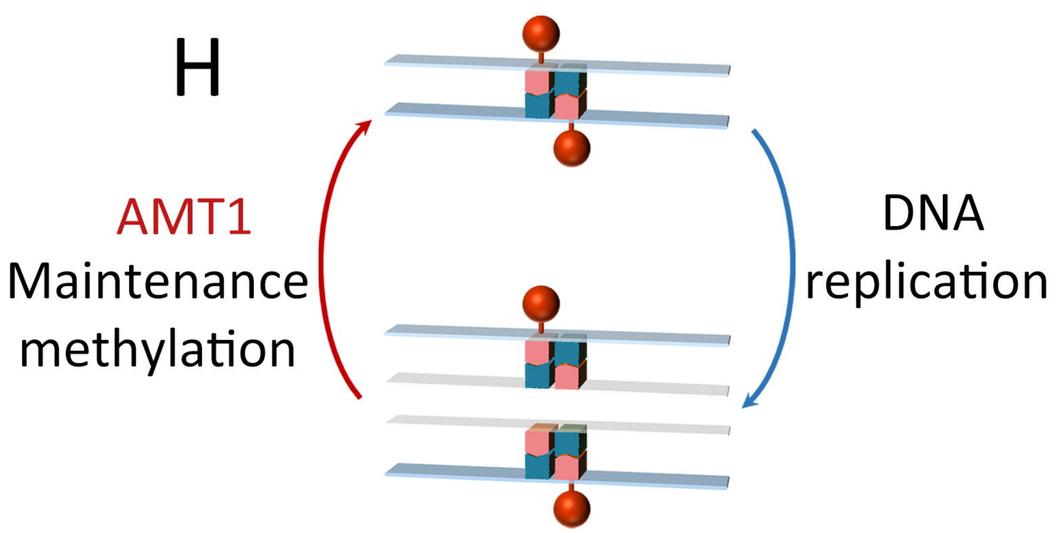
AMT1
Maintenance methylation
DNA replication

A

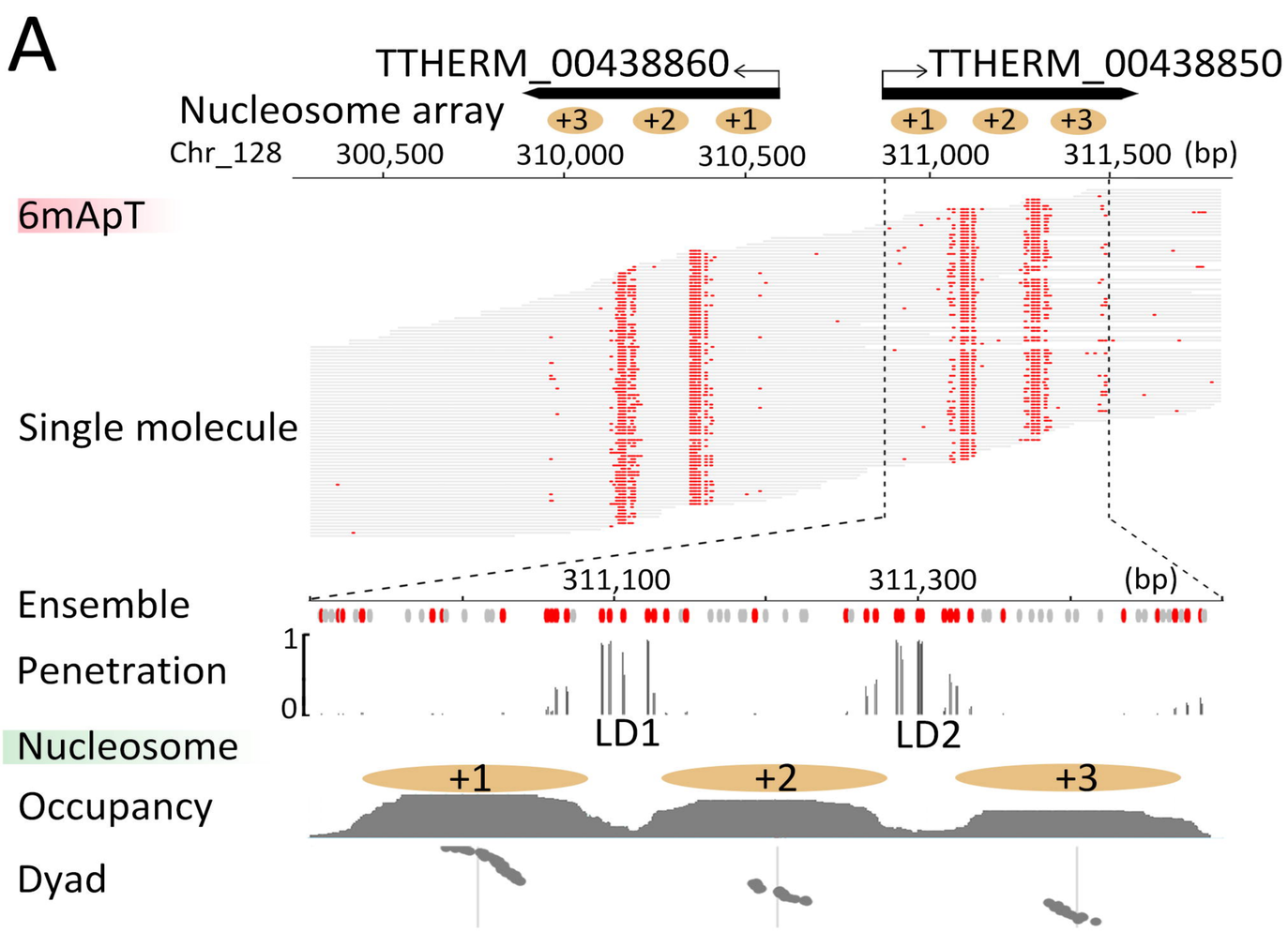

B

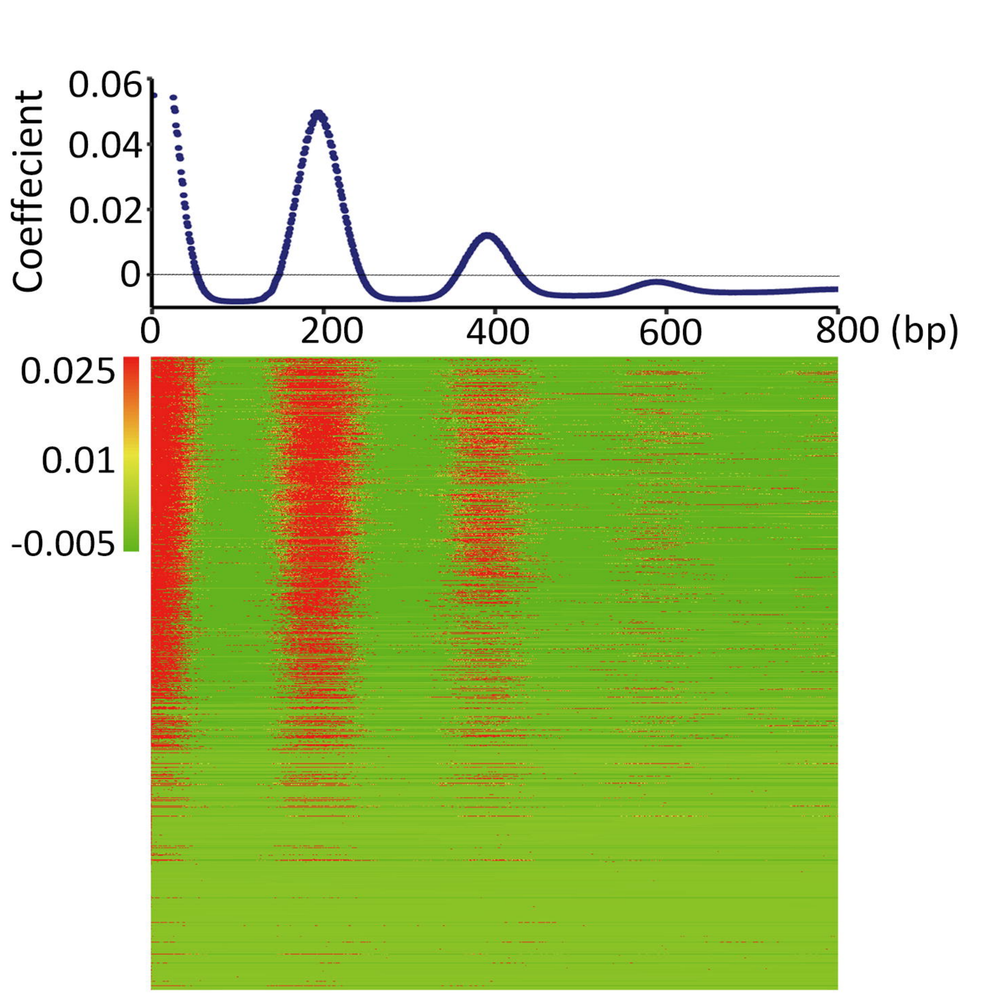

C

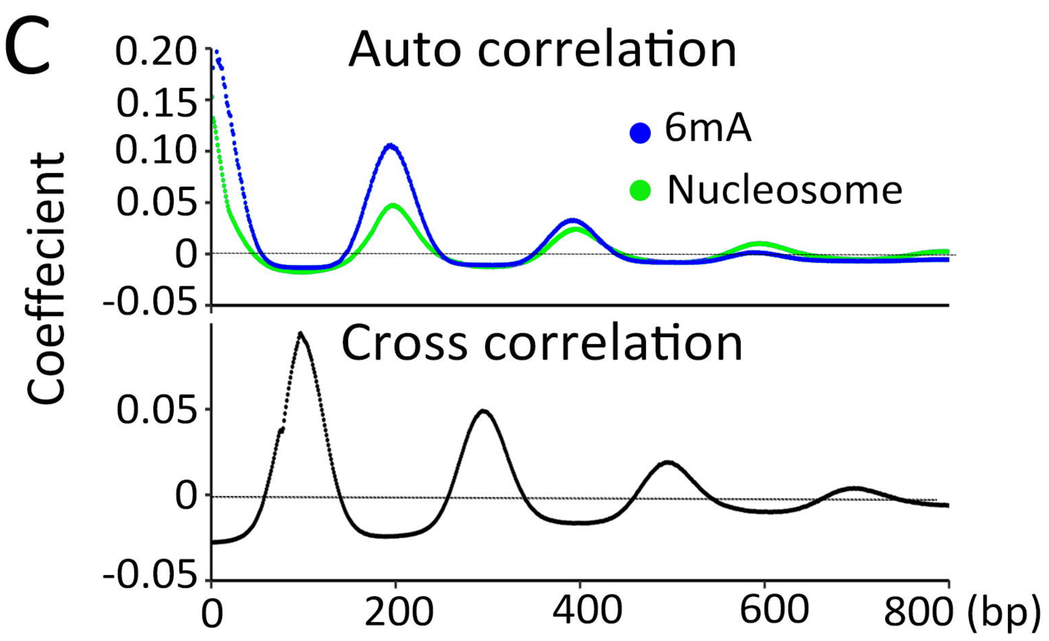

D

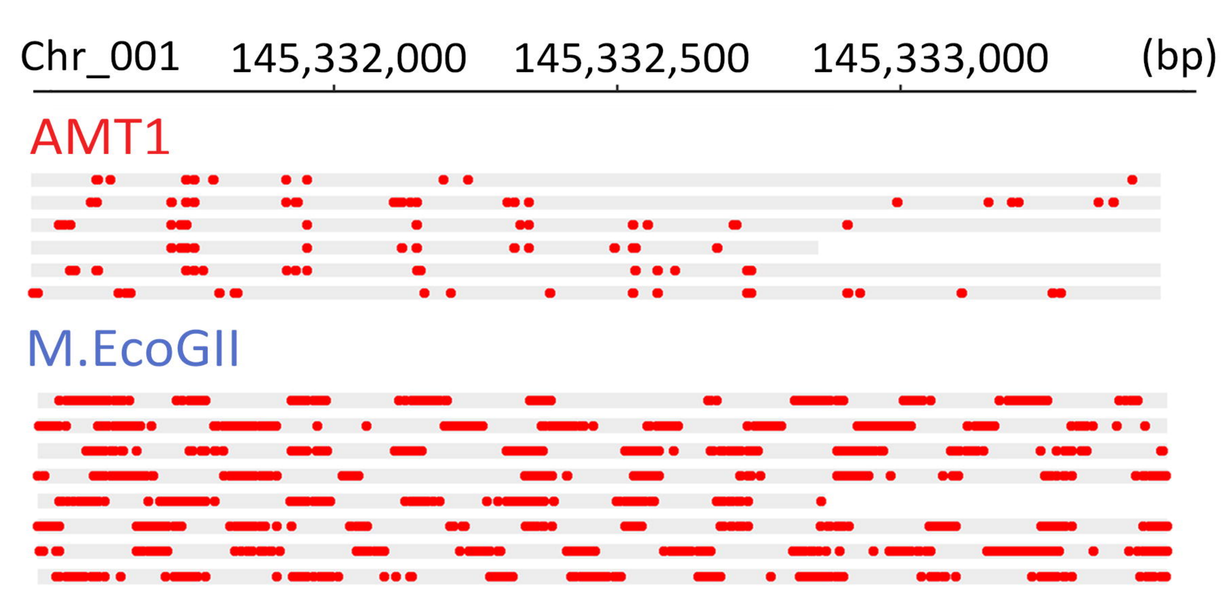

E

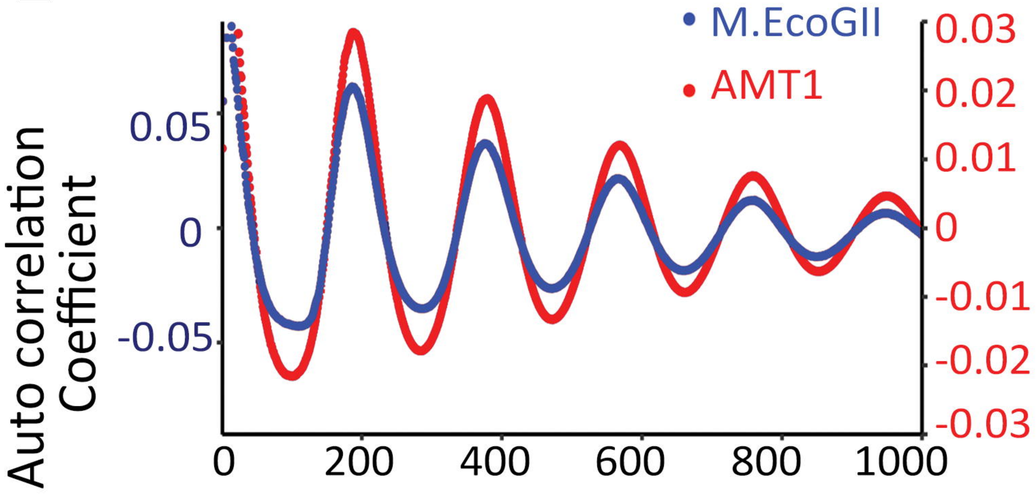

F

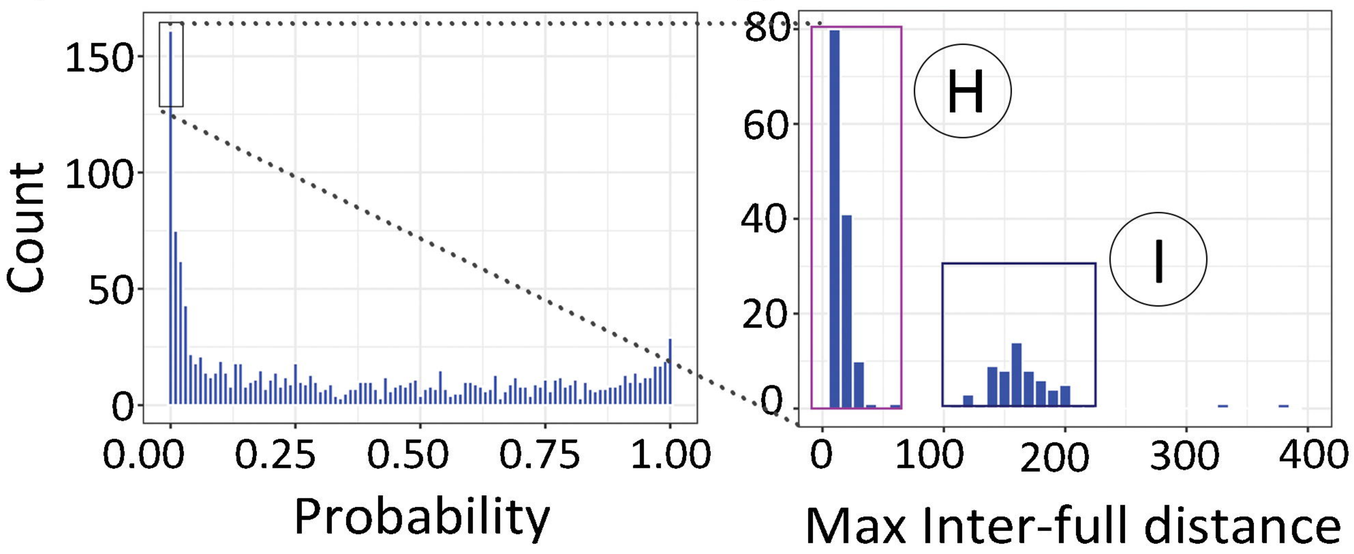

G

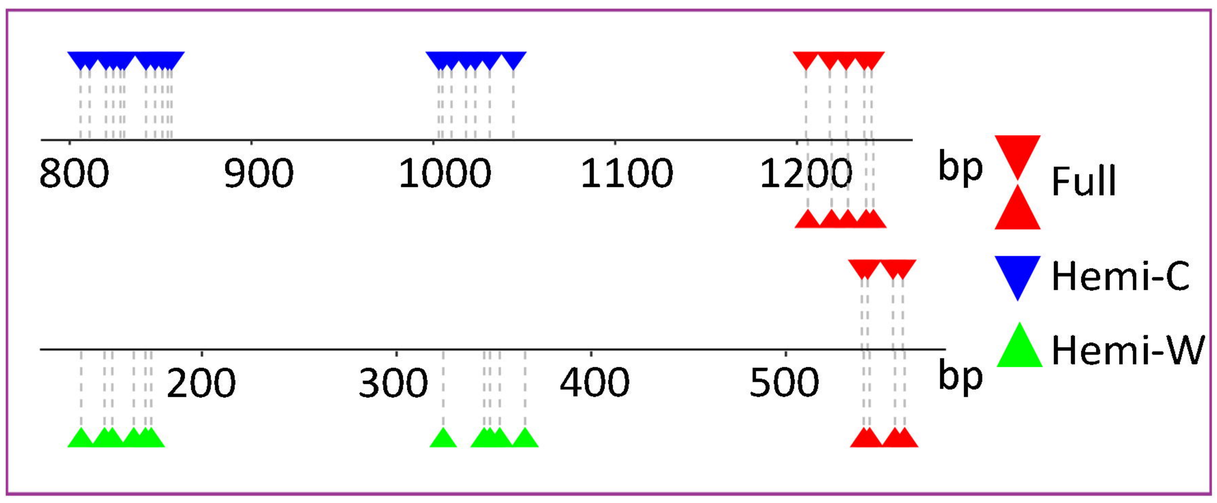

H

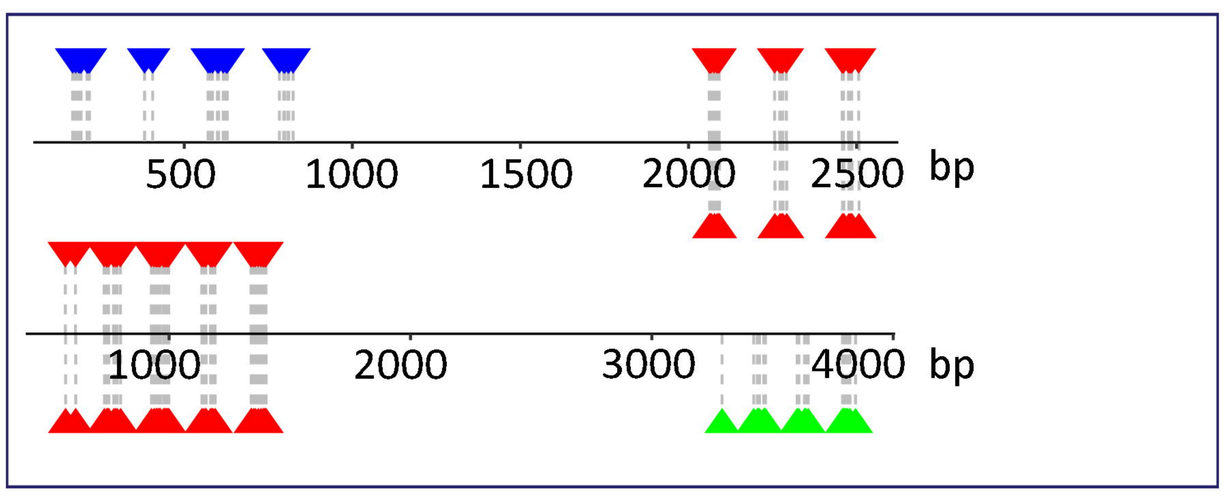

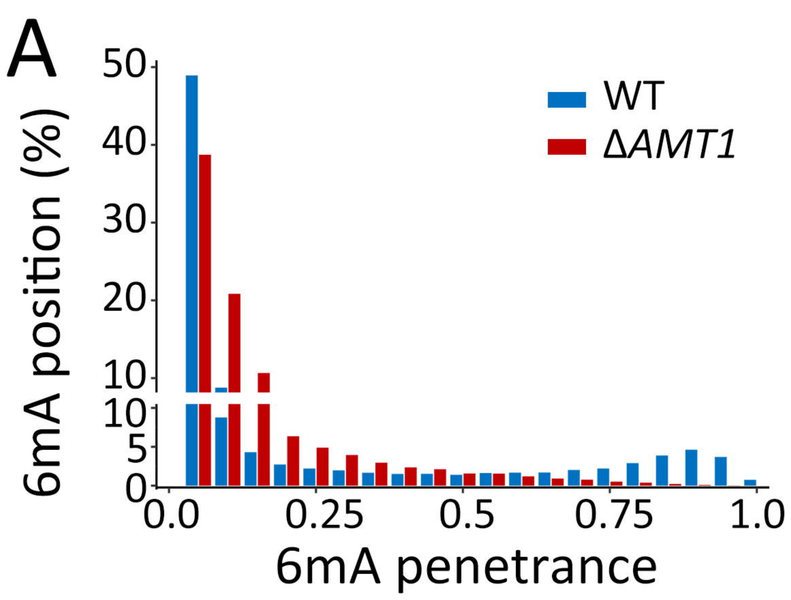
A
6mA position (%)
WT
ΔAMT1
6mA penetrance

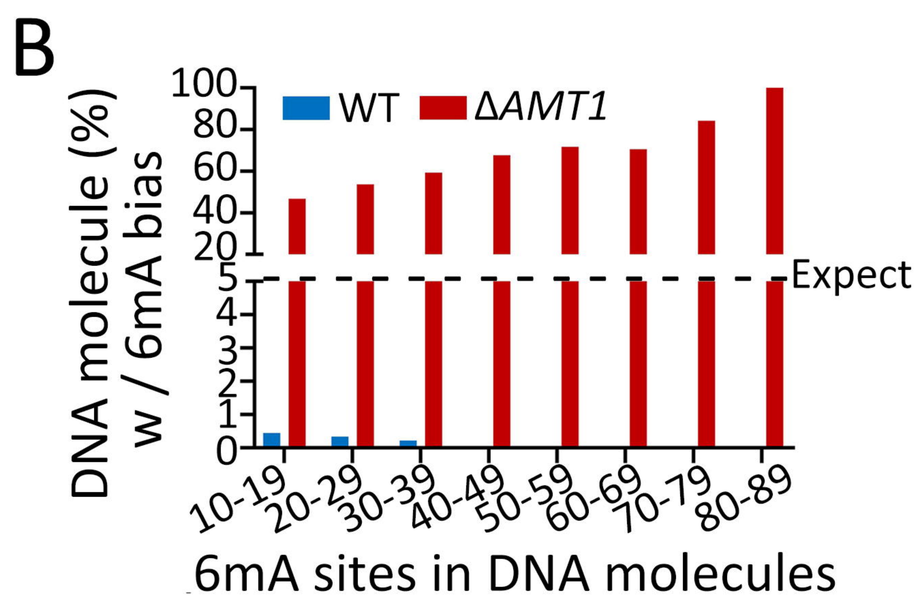
B
DNA molecule (%)
w / 6mA bias
WT
ΔAMT1
Expect
6mA sites in DNA molecules

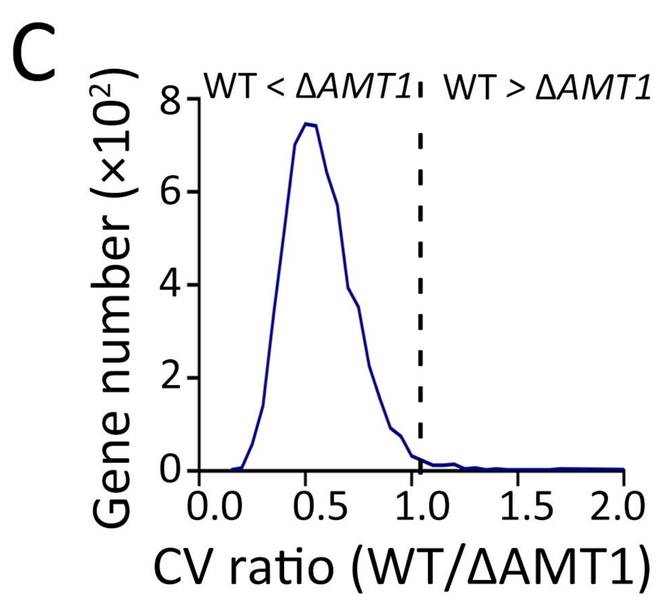
C
WT < ΔAMT1
WT > ΔAMT1
Gene number (×10²)
CV ratio (WT/ΔAMT1)

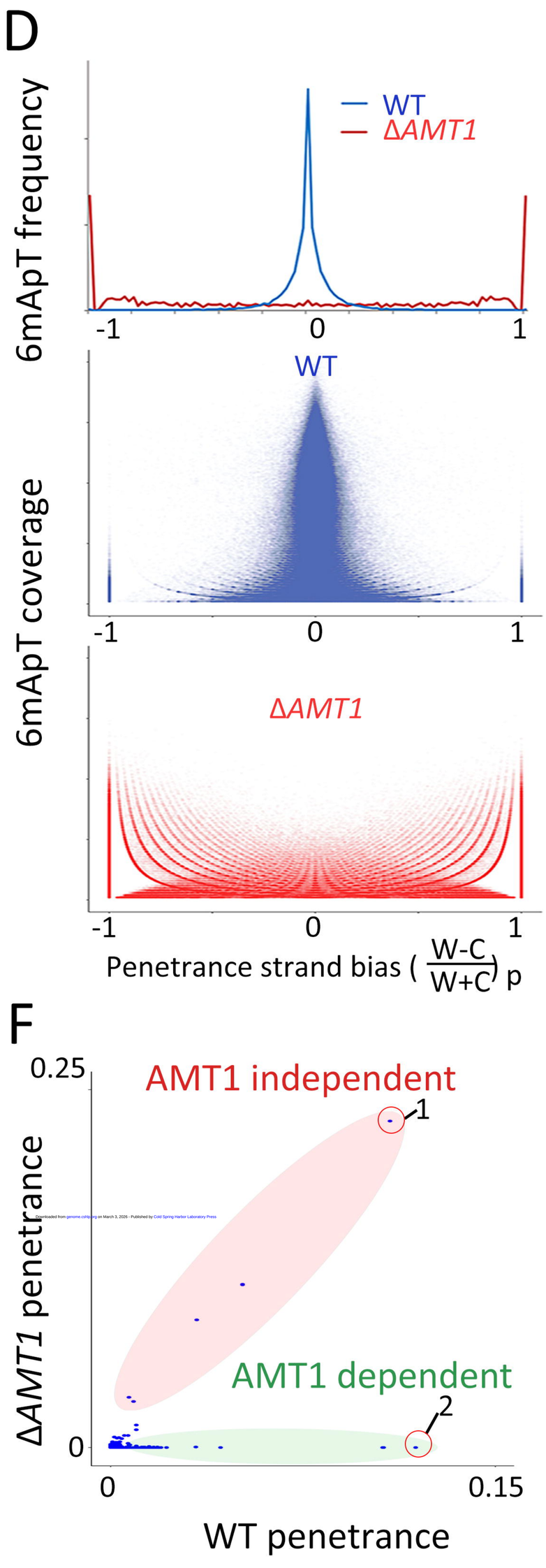
D
6mApT frequency
WT
ΔAMT1
6mApT coverage
Penetrance strand bias (W-C / W+C) p

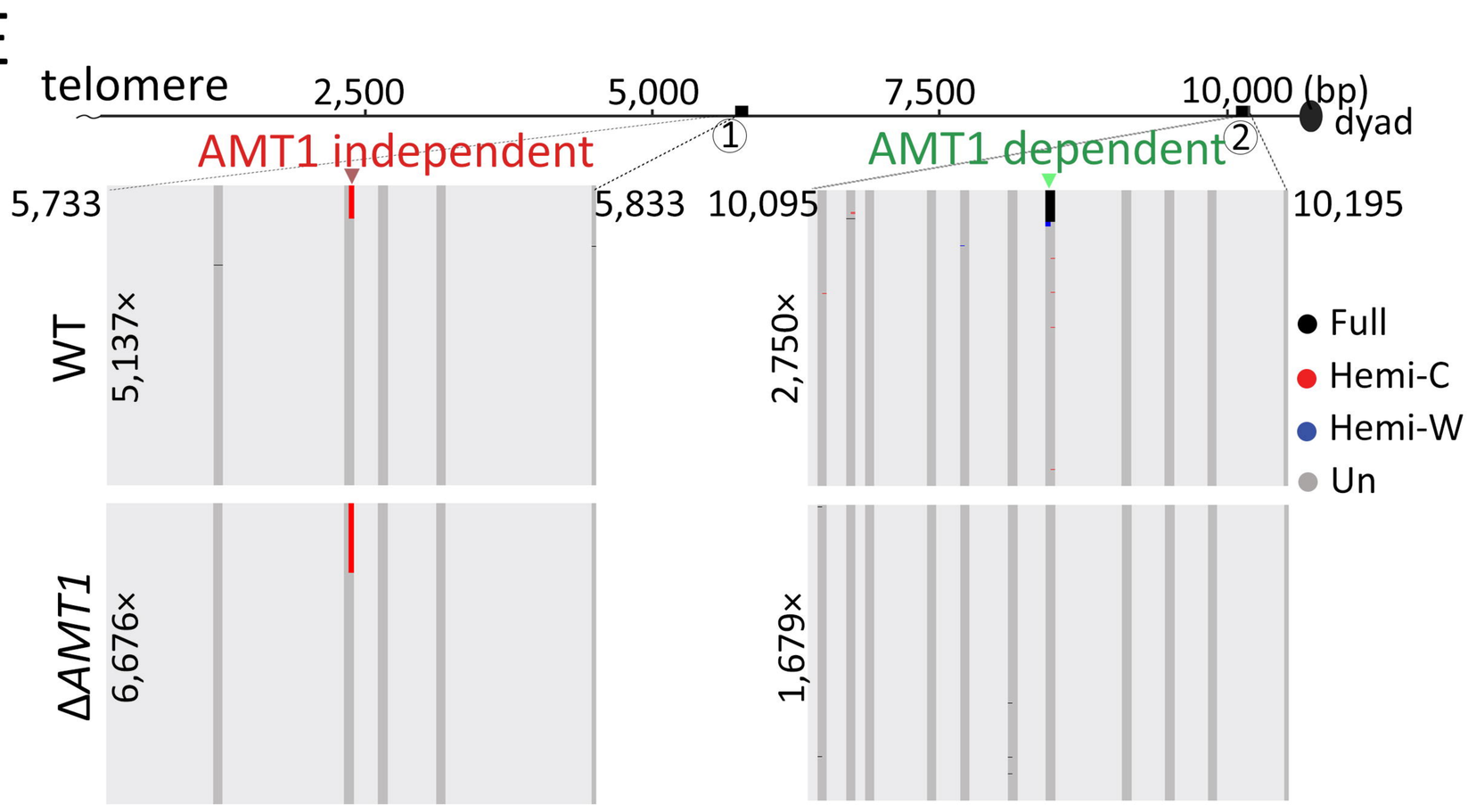
E
telomere
2,500
5,000
7,500
10,000 (bp)
dyad
AMT1 independent
AMT1 dependent
5,733
5,833
10,095
10,195
WT
5,137×
2,750×
ΔAMT1
6,676×
1,679×
Full
Hemi-C
Hemi-W
Un

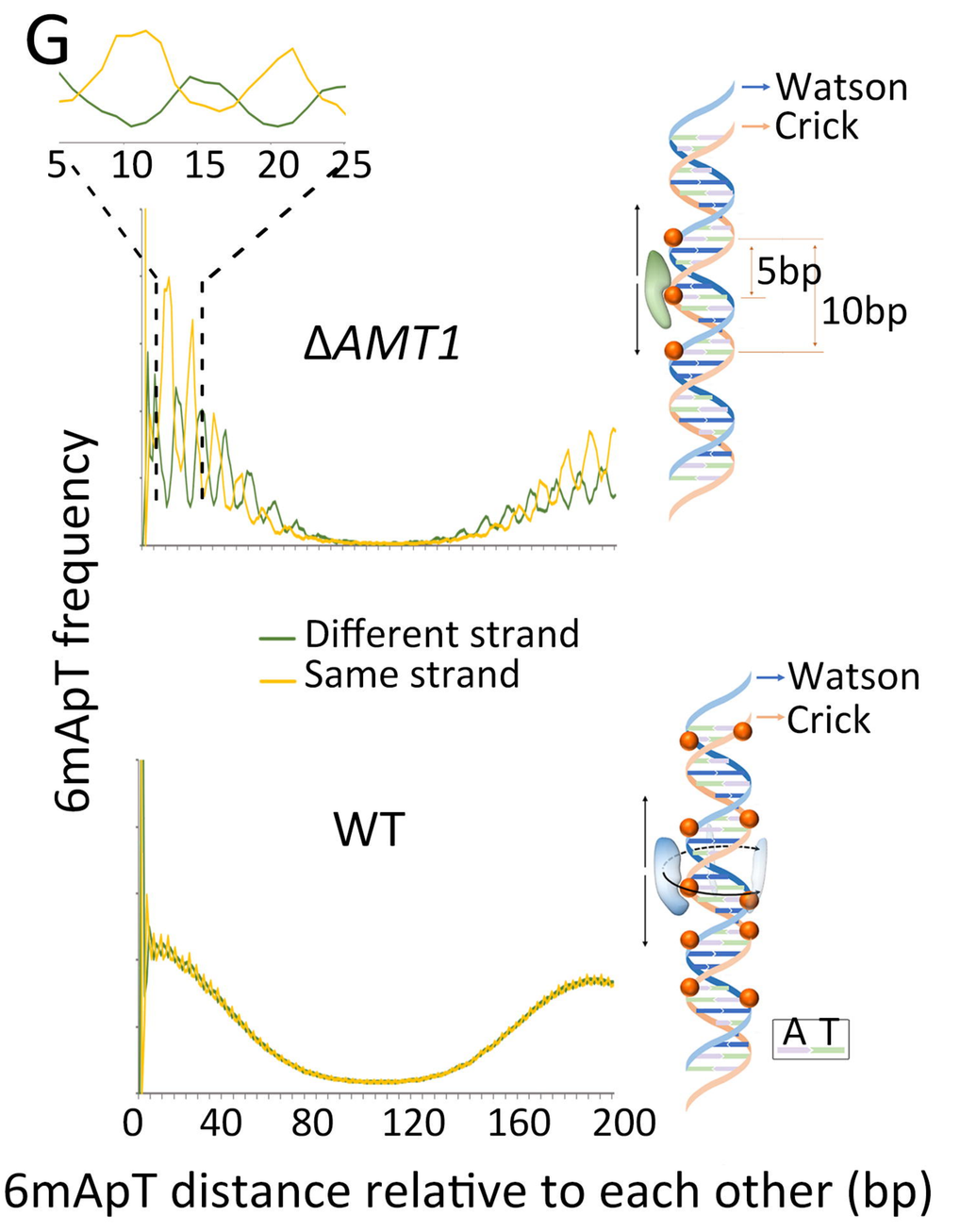
G
6mApT frequency
ΔAMT1
Different strand
Same strand
WT
6mApT distance relative to each other (bp)
Watson
Crick
5bp
10bp
A T

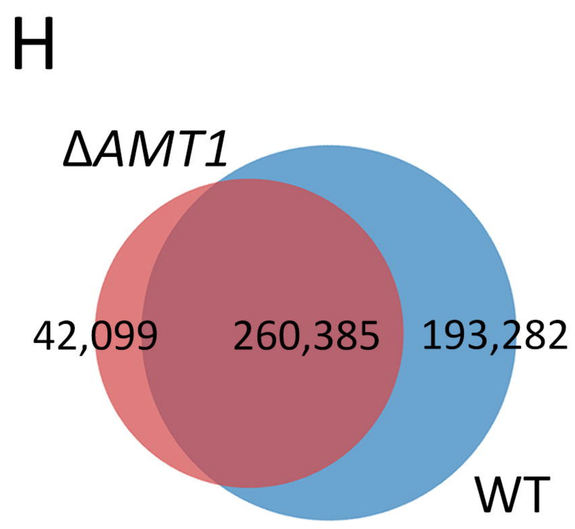
H
ΔAMT1
42,099
260,385
193,282
WT

F
AMT1 independent
AMT1 dependent
ΔAMT1 penetrance
WT penetrance

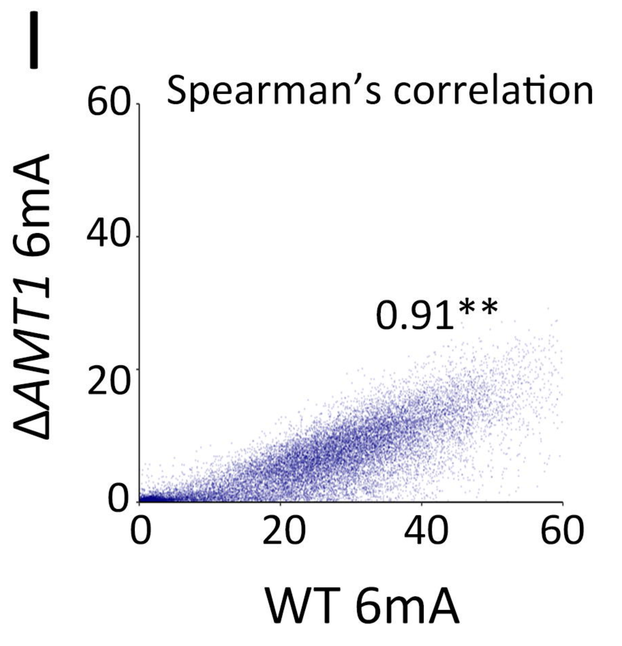
I
Spearman's correlation
0.91**
ΔAMT1 6mA
WT 6mA

6mA

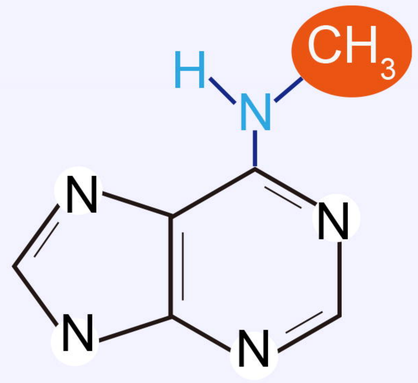

N^6-methyladenine, 6mA

Transcription activation
Lower eukaryotes

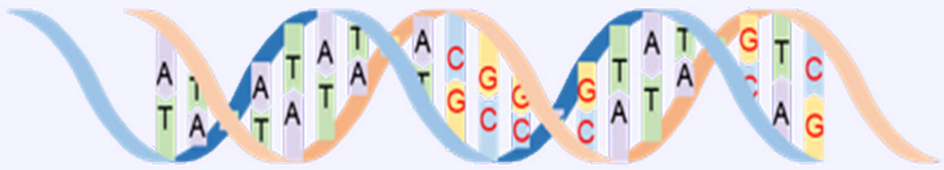

de novo
methylation

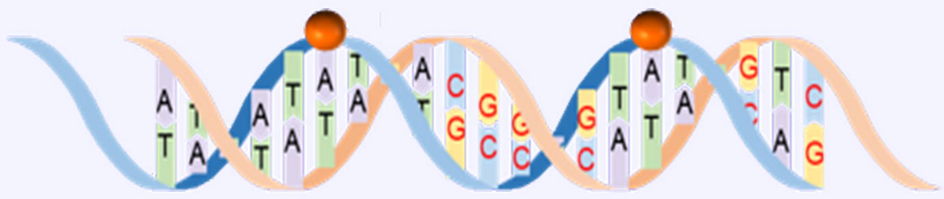

Maintenance
methylation

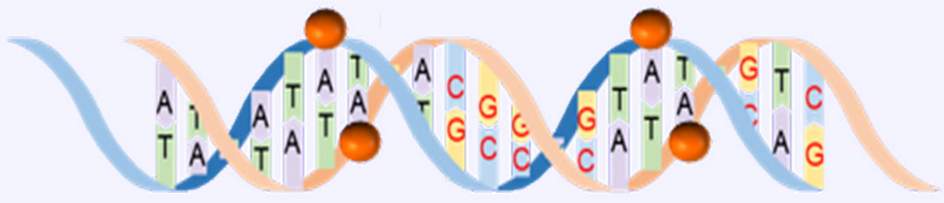

5mC

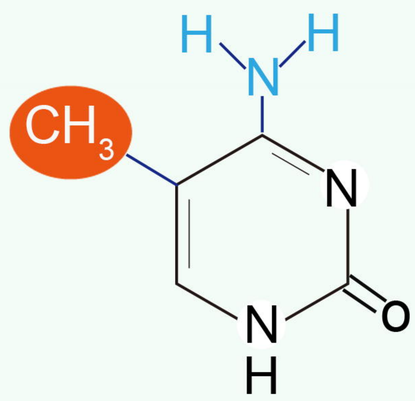

5-methylcytosine, 5mC

Transcription repression
Lower/higher eukaryotes

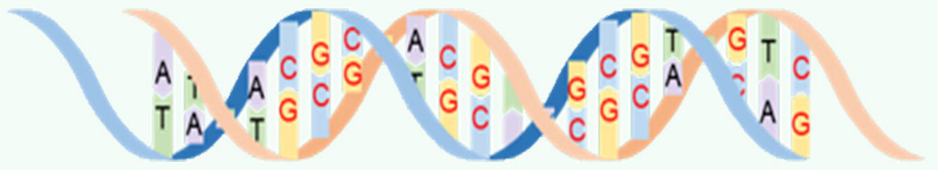

DNMT3A/3B

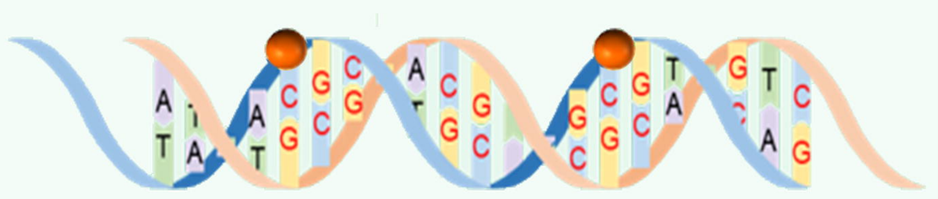

DNMT1

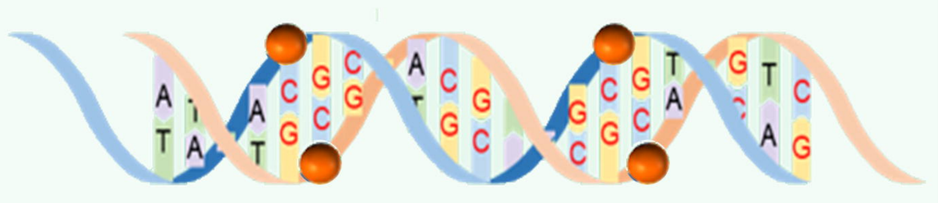

Semiconservative transmission of DNA N6-adenine methylation in a unicellular eukaryote

Yalan Sheng, Yuanyuan Wang, Wentao Yang, et al.

Genome Res. published online May 14, 2024
Access the most recent version at doi:10.1101/gr.277843.123